Nanoscale

Accepted Manuscript

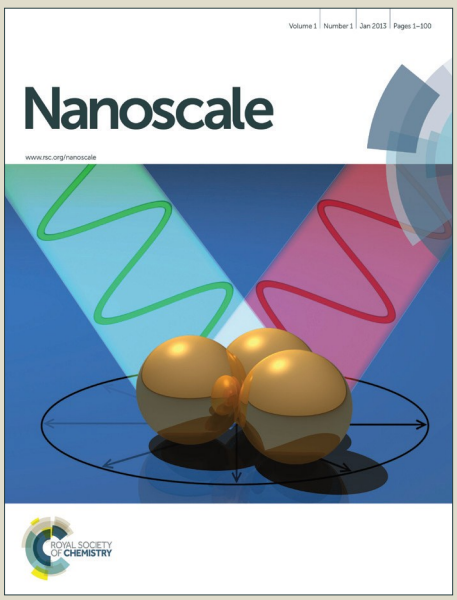

ROYAL SOCIETY OF CHEMISTRY

www.rsc.org/nanoscale

Atomistic modeling of BN nanofillers for mechanical and thermal properties: a review

Rajesh Kumar and Avinash Parashar*

Department of Mechanical and Industrial Engineering
Indian Institute of Technology, Roorkee - 247667, India
* Corresponding author: E-Mail: drap1fme@iitr.ac.in, Ph.: +91-1332-284801

ABSTRACT

Due to exceptional mechanical properties, thermal conductivity and wide band gap (5-6eV), boron nitride nanotubes and nanosheets have promising applications in the field of engineering and biomedical science. Accurate modeling of failure or fracture in a nanomaterial inherently involves coupling of atomic domains of crack, voids as well as deformation mechanism originating from grain boundaries. This review highlights the recent progress made in the atomistic modeling of boron nitride nanofillers. Continuous improvements in computational power have made it possible to study structural properties of these nanofillers at atomistic scale.

Keywords: Boron nitride; nanofillers; finite element; density functional theory; molecular dynamics; Tersoff potential; hybrid nanostructures

1.0 Introduction

Boron nitride (BN) is a lab-grown binary compound consisting of equal number of boron (B) and nitrogen (N) atoms. BN crystallizes either as a hexagonal layered structure or as a tetrahedral linked structure, similar to those of graphite and diamond respectively. Due to white color and slippery properties hexagonal boron nitride (h-BN) is also known as white graphite or graphitic

boron nitride [1, 2]. In 1995, BN was first synthesized as boron nitride nanotubes (BNNT) and in continuation to that work, BN nanomeshes were further developed [3].

Similar to carbon based nanofillers e.g. graphene and carbon nanotubes; BN nanotubes (BNNT) and nanosheets (BNNS) also have hexagonal closed packed atomic configuration [4-6]. BN nanofillers (BNNT or BNNS) exist in hexagonal form with alternatively placed boron (B) and nitrogen (N) atoms as illustrated in **Fig. 1**. Despite similar atomic configurations, comparable mechanical and thermal properties [7-8], BN nanofillers are good electric insulators [1, 9-10] as compared to corresponding carbon based nanofillers.

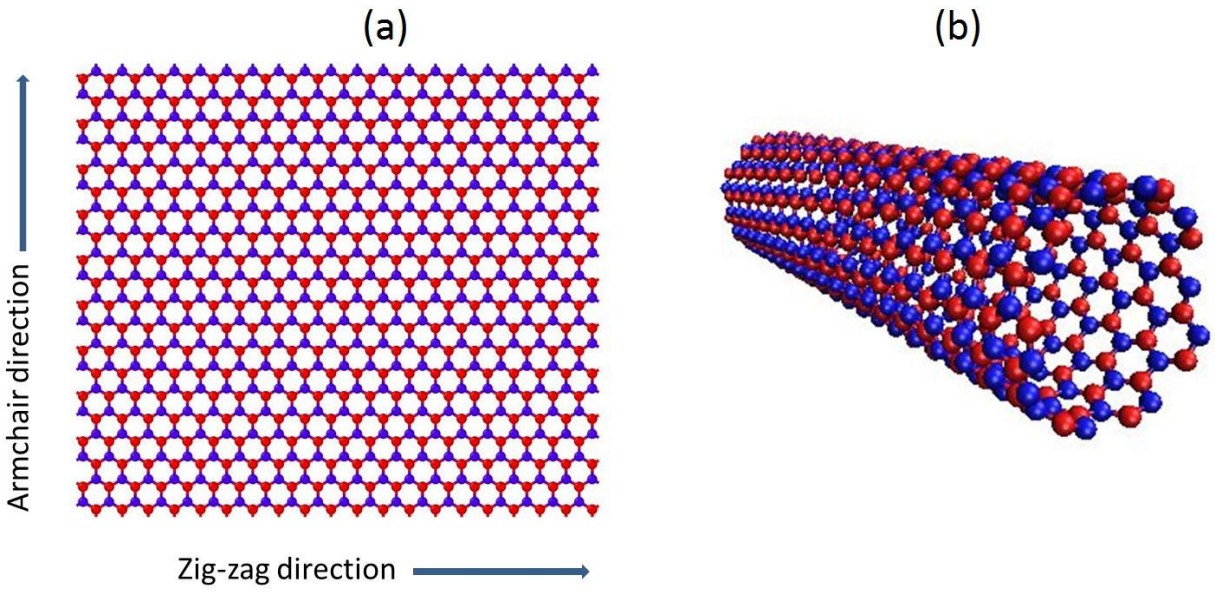

Fig. 1. Atomic configuration of (a) Single layer BNNS (b) Single-walled BNNT. Red and blue dots correspond to boron and nitrogen atoms, respectively**.**

Due to wide band gap, h-BN is preferred over graphene for specific applications such as electronic packaging [11-14]. In addition to exceptional mechanical properties [15-26], thermal conductivity [27] and electrical insulating properties [1, 9-10], BN nanofillers are also highly

stable against oxidation even at very high temperatures such as 800°C [28]. At such high working temperatures, BN nanofillers are considered chemically and structurally more stable as compared to corresponding carbon based nanostructures [28-29]. Thermal conductivity of BN nanofillers has been reported in the range of 1700-2000 W m^{-1} K^{-1} [27]. In addition to these exceptional properties, BN nanofillers have also shown deep ultraviolet photon emission [30], and a good amount of piezoelectricity [31-33].

Due to the above mentioned exceptional properties, h-BN nanofillers have found applications in many areas such as nano-sensors [34-39], bio-sensors [34-37, 39], biomaterials [40-42] and in developing corrosion-resistant and thermally stable composites [43-49]. Bio-compatibility, biosafety and high hemo/histocompatibility of BN nanofillers are promoting researchers to use them as therapeutic agents to treat neuro-genetic disorders [50-55]. Neutron absorption capacity of these nanofillers has also found applications in the field of cancer treatment such as cerebral gliblastoma multiforme [56]. Adsorption of hydrogen on the surface of BNNTs and BNNSs [57-59] also opens the door for hydrogen storage at ambient temperature. Some other prominent applications of BN nanofillers include optoelectronics [60-66] and tribology [67-69]. Due to their excellent sorption capabilities for a wide range of oils, solvents and dyes, their application has also been proposed to be used as a water purifier [70].

Despite the availability of high yield synthesis techniques [71], commercial production of these nanofillers is still in an immature state, due to limited availability of techniques for characterizing these nanofillers. Due to challenges associated with the characterization of these BN nanofillers, limited research has been published in this area as compared to that of carbon based nanofillers. A year wise comparative chart for the number of publications in the field of respective nanofillers is plotted in **Fig. 2**.

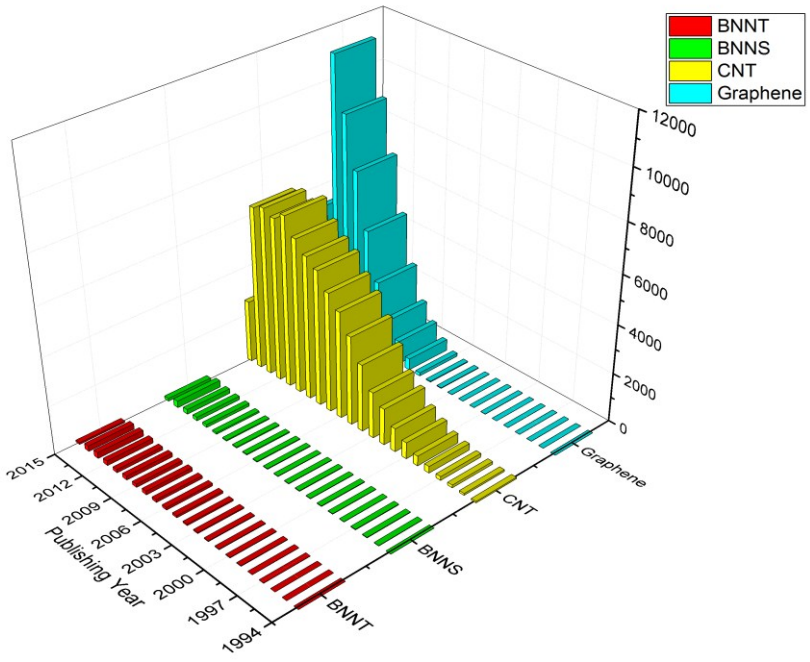

Fig.2. A year wise graphical comparison of research papers published and containing respective phrases i.e. BNNT, BNNS, CNT & Graphene in their title. Statistics based on Scopus database, as of June 15th, 2015.

There are a number of methods that are currently being used for the production of h-BN nanofillers. Monolayer to few-layers of h-BN flakes can be exfoliated from bulk BN crystals either by mechanical cleavage/exfoliation [72-73] or by chemical-solution-derived method [74]. Other synthesis methods for BN nanofillers include chemical vapor deposition (CVD) [75-79], sonication [80-81], ball milling [81-82], high-energy electron beam irradiation [83-84], reaction of boric acid and urea [85-86], metal-catalyst-free approach [87], chemical blowing (mass production technique that relies on generating large bubbles of BNH or BNCH from a precursor ammonia borate compound)[88-89], using substitution reaction [90-91], via micro-fluidization [92] and via laser ablation [93-96]. The electrical insulating property that singles out BN nanofillers from other nanofillers has been extensively studied by researchers. In 1994, Blase et al. [9] predicted a constant band gap for BN nanotubes and this was further explored by

Watanabe et al. [10] to establish the fact that BN nanotubes have a direct-band gap in the ultra-violet region. Zhang et al. [97] predicted the stability and electronic structure of BNNTs with diameters below 0.4 nm. In their work on BNNT's numerical based techniques have been used to study the effect of nanotube diameter, chirality and multiwall BN structures on the band gap or electrical insulation. These exceptional properties, along with diversified field of applications have developed keen interest in the researchers to explore more about these nanofillers. Starting from 1994, researchers are trying to study BN nanofillers using different techniques such as experiments, finite element based continuum models, molecular dynamics based atomistic models, and higher fidelity numerical simulations such as density functional theory (DFT).

So far, only a limited number of review papers have been published on BN nanofillers, and most of them are focused on the generalized topics. Atomistic modeling techniques are emerging as the focused area of research for researchers to investigate the behavior of these nanofillers. The aim of the present article is to address the current state of art in simulating the mechanical as well as thermal behavior of BNNS and BNNT with the help of atomistic modeling based approaches. Authors have also attempted to illustrate the challenges associated with each kind of atomistic modeling technique.

2.0 Atomistic Modeling Techniques

During the last couple of years, several experimental and modeling techniques have been employed by the researchers to characterize or predict the mechanical and thermal behavior of BN nanofillers. Despite the fact that experimental techniques are costly and time consuming, experiments are still considered as a realistic tool for characterizing the behavior of materials. Transmission electron microscope (TEM) [15-16, 23-24, 85, 98] and atomic force microscope

(AFM) based techniques [15-16, 73, 99] are usually employed in experimental characterization of nano materials. In addition to these common techniques, x-ray based scattering has also been employed for estimating the five elastic moduli of h-BN [100].

In addition to cost and time involved, experimental techniques also have some limitations in estimating the localized mechanical or thermal behavior of these nanofillers at the atomistic level. Due to these limitations associated with experimental techniques, computational techniques based on finite element, DFT and MD are emerging as effective tools to predict the mechanical as well as thermal behavior of these nanofillers. Atomistic simulations are not substituting experiments but are complementing them at nanoscale.

2.1 Structural Mechanics Based Approach

The theoretical approaches, mentioned above, can be further classified as atomistic and continuum based approaches. The atomistic approaches include classical molecular dynamics and density functional theory, whereas the continuum mechanics based approach mainly consists of classical continuum mechanics and shell modeling [101-103]. The structural mechanics based approach developed and proposed by Li and Chou [104] is considered as a pioneer research in the field of atomistic modeling of nanofillers. Their model was based on the notion that the nanofillers (e.g. CNT) are geometrical space frame structures and can be studied with the help of structural mechanics. In structural mechanics based approach atomic nuclei are treated as material points. The motion of atomic nuclei is regulated by a force field and this force field is generally expressed as the steric potential energy which depends on the relative position of atomic nuclei. In 2005, Tserpes and Papanikos [105] implemented the concept of Li and Chou [104] in finite element method (FEM). In their FEM based approach, bonds are simulated as load

carrying elements, and atoms as joints or nodes for connecting these elements as illustrated in **Fig. 3**. In FEM based approaches the material properties or stiffness matrix is generated by establishing a linkage between molecular and continuum mechanics.

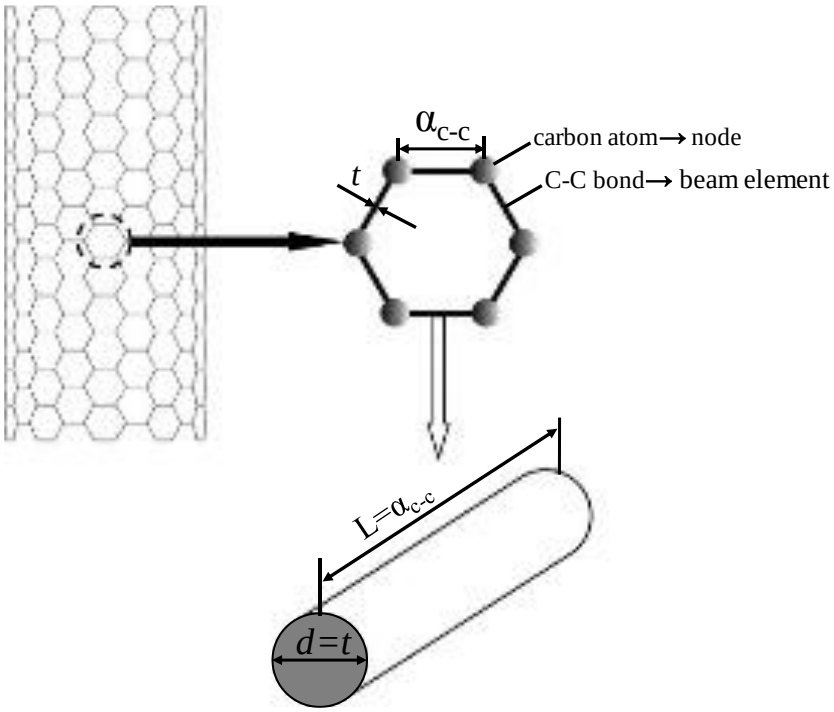

Fig. 3. Schematic of space frame model for CNT (Reproduced with permission from [105])

Harmonic, Morse and Lennard Jones LJ 6-12 (van der Waals) like interatomic potentials are commonly employed in FEM based models for generating the stiffness matrix. These interatomic potentials account for all the bonded as well as non-bonded interactions. These structural mechanics based modeling techniques have also been extended by researchers for the modeling of BN nanofillers [106-108]. In 2011, Boldrin et al. [106] extended the space frame models for the simulation of h-BN nanosheets. They employed molecular mechanics in conjunction with finite element to study the effective mechanical properties of h-BN nanosheets. In addition to these space frame based atomistic models, continuum based lattice approach has also been

employed in conjunction with Tersoff-Brenner potential for estimating the Young's modulus and Poisson's ratio of boron nitride crystals [109]. Numerical techniques, based on the sub-hexagonal lattice- sums [110], have been further extended by Green et al. [111] to study the elastic behavior of h-BN. Finite element based continuum models are considered suitable for predicting the average or the global properties of these nanofillers.

2.2 Density Functional Theory (DFT)

Density Functional Theory (DFT) is a quantum mechanics based higher fidelity simulation technique, and is common among the researchers for estimating the atomic level properties of materials in physics, materials science and chemistry. In DFT, atomic nuclei are usually treated as frozen while electrons are considered to be moving in the electrostatic field generated by the nuclei (Born–Oppenheimer approximation). In DFT based atomistic simulations, electron density is used as its central part to calculate the total energy of the system. This energy E[ρ] is a functional of electron energy density 'ρ' and is expressed as:

$$E[\rho] = T[\rho] + E_H[\rho] + E_{xc}[\rho] + E_{ext}[\rho] + E_{zz} \quad \textbf{(1)}$$

Where T[ρ], E_H[ρ], E_{xc}[ρ], E_{ext}[ρ] and E_{zz} are energy contributions from kinetic energy of non-interacting electrons, Hartree energy, exchange-correlation energy, external potential (here due to potential of nuclei) and ions energy due to interaction among nuclei, respectively. Kohn–Sham method is the most widely used DFT technique in which rather than finding a solution for electron wave functions a solution for electron density functional is sought. Based on Kohn-Sham theory, a system of many interacting particles is converted to an equivalent fictitious

system of non-interacting particles. Kohn-Sham (KS) equations for this new system model are given by **Eq. (2)** and **(3)**.

$$\left[-\frac{1}{2}\nabla^2 + V_{eff}(r)\right]\phi_i(r) = \epsilon_i\phi_i \quad \textbf{(2)}$$

Where

$$V_{eff} = \frac{\delta(E_H[\rho] + E_{xc}[\rho] + E_{ext}[\rho]}{\delta\rho} = V_H[\rho] + V_{xc}[\rho] + V_{ext}[\rho] \quad \textbf{(3)}$$

and is known as Kohn-Sham or effective potential, ϕ_i are the Kohn-Sham one-electron orbitals whereas electron density *ρ(r)* is given by:

$$\rho(r) = \sum_{i=1}^{N} |\phi_i|^2 \quad \textbf{(4)}$$

Due to Kohn-Sham formulations, the multi-electron problem is reduced to seeking a set of solutions to one electron problems. For solution of the equations, an initial guess of electron density "ρ" is made and is used for further calculations. For solving the Kohn-Sham equations, two types of basis sets "atomic orbitals" or "plane wave" are usually used by researchers. In the first case, a linear combination of atomic orbitals (LCAO), such as Gaussian orbitals, is used. LCAO is especially suitable for study of molecules or systems with strong directional bonding. But non-orthogonal nature of these orbitals makes the calculations complex and creates practical inconvenience in the way that there is no systematic way that improves accuracy if the number of basis sets are increased. The other common basis set i.e. plane wave, is good for periodic systems (such as solids) but can also be adapted for finite size systems, such as atoms or molecules, with

supercell approach where large periodicity of simulation box is ensured. The plane wave basis sets are usually used for valence space in conjunction with pseudopotentials.

Before solving Kohn-Sham equations, all the energy terms in the equations need to be evaluated. Except exchange-correlation energy, all other energy terms can be estimated easily. Exchange-correlation energy is usually estimated by using some approximations such as local density approximation (LDA) [112(PW92)-113(PZ81)], generalized gradient approximation (CGA) [114(PBE)-115(LYP)] etc. LDA is the simplest one and neglects the gradients in electron density. Despite being simple, LDA gives quite good results even with this simple approach. Other approximations include meta-CGA [116(TPSS)], hybrid functional [117-118(PBE0)] and some meta-hybrid functionals and the choice out of them is application specific.

For solid state systems, a suitable method is to use the pseudopotential (PP) approach. In this method, interactions between core electrons and valence electrons are treated with pseudopotential function. Pseudopotential approach is based on the consideration that core electrons do not participate significantly in the bonding process and can be neglected while solving for electronic structure of the electrons. On the other hand, valence electrons, which are fewer in number, are treated with plane-wave basis sets. Although high in number, but plane-waves are used in the solids because they are cheap to compute. Pseudopotentials may be an empirical pseudopotential or *ab initio* pseudopotential. *Ab initio* pseudopotentials based on local solutions of wave functions near the atomic nuclei are commonly preferred over the empirical pseudopotentials. However, in more accurate DFT implementations, non-local form of pseudopotentials is used.

The pseudopotential approach is much faster than all-electron calculations because tightly-bound core electrons are not directly taken into the account for calculations. After solving KS equations, output electron density obtained is used to calculate the total ground state energy of the whole system. This procedure is repeated until a self-consistent solution is achieved. This optimized total ground state energy is further used to estimate the other structural properties of the material. An overview of DFT process has been shown in **Fig. 4.** While solving KS equations construction of density matrix from Fock/Kohn-Sham matrix and then solving for density functional is an expensive process which makes DFT a computationally intensive technique. However, another approach based on DFT, which is faster with surprisingly good accuracy, is tight-binding (TB) method in which valence electrons are treated 'tightly bound' to its nucleus and atomic orbitals are not altered during bonding process. The tight-binding model is based on the set of approximations obtained from quantum mechanics and hence is less computationally intensive. Even though this method is less accurate as compared to *ab initio* DFT but is sufficiently accurate for the structures to which it is fitted. The method is usually applied to covalent system such as semi-conductors (Si, Ge) and to carbon. In DFT calculations, mechanical properties are estimated using strain energy (U) obtained by the following equation:

$$U = U_{\varepsilon} - U_{\varepsilon=0} \quad \textbf{(5)}$$

Where, U_{ε} and $U_{\varepsilon=0}$ are the potential energy of the strained and unstrained atomistic system respectively.

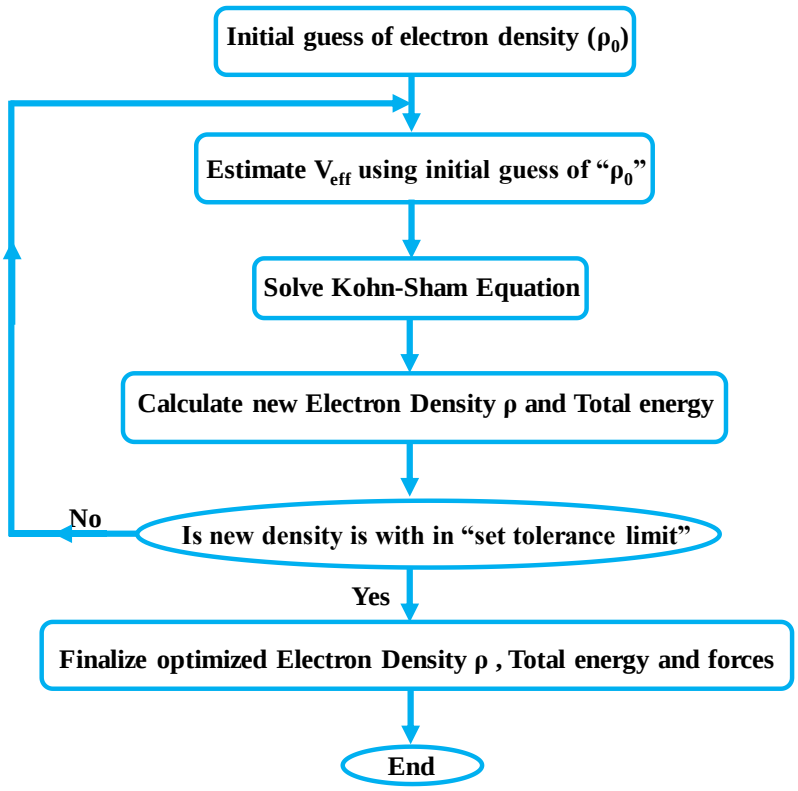

Fig. 4. An overview chart of iterative DFT process.

The value of strained energy is further processed to calculate the Young's modulus (Y in N/m^2) and 2D Young's modulus (Y_S in N/m) as illustrated in **Eq. (6)** and **(7)** respectively:

$$Y = \left(\partial^2 U / \partial \varepsilon^2\right) / V \quad \textbf{(6)}$$

$$Y_s = \left(\partial^2 U / \partial \varepsilon^2\right) / S \quad \textbf{(7)}$$

Here, V is the volume and S is the surface area of the system.

With BN nanofillers, DFT and other DFT based approaches have also been used by researchers to estimate the elastic as well as other structural properties [17-20, 25, 119-123]. Kudin and

Scuseria [17] employed DFT with Gaussian type's orbitals and PBE [114] approximations to study the elastic behavior of BNNT. They predicted an average value of nearly 810 GPa for Young's modulus of the nanotubes which was in close agreement with tight-binding calculations of Hernandez et al. [124]. Later on, Suryavanshi et al. [24] also reported a value of nearly 722 GPa for Young's modulus of BNNTs using experimental techniques. In 2009, Sahin et al. [18] used DFT framework to investigate the elastic and other properties of BN nanosheets. A combination of first-principles plane-wave calculations and projector augmented wave potentials [125] was used to ensure accuracy and computation speed. They predicted a value of nearly 810 GPa (assuming a thickness of 0.33 nm for BNNS) for Young's modulus which was close the value reported by Bosak et al. [100] using inelastic x-ray scattering measurements. Some more works [19-20, 126] performed in DFT framework also predicted nearly close values of Young's modulus to the studies mentioned previously in this paragraph. A combination of DFT and quasi-harmonic approximation (QHA) [127] was successfully applied by researchers [128] to evaluate the effect of temperature on mechanical behavior of BN nanosheets. It was found that Young's modulus of boron nanosheets nanotubes increases with increase in temperature up to a temperature of 800^0 C. After this temperature, the rate of increase was slow and temperature tended to a constant value.

Although, DFT based approach has been successfully applied for the atomistic modeling and predicting properties of materials quite accurately yet it has certain limitations associated with it. As already mentioned generally it is considered computationally intensive and can only be performed with limited number of atoms. Tight-binding methods are considered good for computational point of view but these have issue of transferability to other systems and even have the issue of number of atoms. Moreover, DFT based approaches are very useful for

developing new empirical interatomic potentials for empirical methods like molecular dynamics. These empirical potentials are considered as the back bone for the less computational intensive molecular dynamics based simulations.

2.3 Molecular Dynamics (MD)

As discussed above, FEM and DFT based approaches have been applied with pretty much success in atomistic modeling, but still have certain limitations. As compared to FEM and DFT based atomistic modeling technique, molecular dynamics (MD) based approach is emerging as yet another alternative to perform atomistic simulations.

MD is a widely used computer based technique for atomistic simulation of atoms/molecules in the context of N-body simulation or many body systems [129]. In MD based simulations atoms are treated as classical particles. Atomic position and potential energy of the system help in computing the atomic forces that are further used in Newton's equation of motion. Relationship derived from the Newton's second law of motion is used for updating the position, velocity and acceleration of each atom in the system at integrated time step. The fundamental equation solved in molecular dynamics based simulation is given as:

$$m_\alpha a_\alpha = F_\alpha = -\left(\partial E / \partial r_\alpha\right) \quad \textbf{(8)}$$

$$\text{where} \quad \alpha = 1, 2, \ldots, N$$

Here, N is total number of atoms; m_α, r_α and F_α are mass, position and time dependent force acting on it due to external agents, respectively. The potential energy 'E' consists of an internal part (E^{int}) that accounts for the interaction between the atoms and an external part (E^{ext}) that accounts for external fields and constraints. Potential energy (E) and hence force F_α are the

functions of position and velocity vectors of the atoms. Statistical mechanics based approaches are commonly used over the time averages to derive macroscopic properties such as pressure, temperature, stresses etc.

In MD based simulations, position and velocity vectors are updated after each time step, usually by using any of the numerical integration algorithms such as Verlet algorithm, Velocity-verlet algorithm [130], Leap-frog algorithm [131], and Beeman's algorithm [132]. But Velocity-verlet algorithm (an extension of Verlet algorithm) is the most widely used integrating scheme in MD based simulations. The position vector '*r*' at any time *t* and after an increment Δt, for any atom involved in the simulation can be expanded as Taylor series expansion as given by **Eq. (9)**.

$$r(t+\Delta t) \approx r(t) + \dot{r}(t)\Delta t + \left(\ddot{r}(t)\Delta t^2\right)/2 + \ldots \quad \textbf{(9)}$$

And, the updated velocity vector after time 't+Δt' can be easily obtained with the help of velocity- verlet equation as:

$$v(t+\Delta t) = v(t) + \left(F(t+\Delta t) + F(t)/2m\right)\Delta t \quad \textbf{(10)}$$

MD simulations are carried out under different types of 'Ensembles'. An ensemble is a collection of all possible different microstates of a system which have an identical macroscopic state. Micro-canonical (NVE), canonical (NVT) and isobaric-isothermal (NPT) are the three most commonly used ensembles in MD simulations.

Most of the interatomic potentials employed in MD based simulations are either derived or developed empirically with the help of experiments or higher fidelity numerical simulations. Interatomic potentials are mathematical expressions for estimating the potential energy (*E*) of the

system of atoms. Commonly used interatomic potentials are Tersoff [133-136], LJ [137], embedded atom method (EAM) [138], REBO [139] and AIREBO [140]. Tersoff type [133-136] interatomic potentials are commonly used for simulating the mechanical and thermal behavior of BN nanofillers. Tersoff potential can be expressed mathematically as given by **Eq. (11)** and **Eq. (12)**:

$$E = \sum_i E_i = \left(\sum_{i \neq j} V_{ij} \right) \Big/ 2, \tag{11}$$

$$V_{ij} = f_c(r_{ij})[a_{ij} f_R(r_{ij}) + b_{ij} f_A(r_{ij})]. \tag{12}$$

Here, E is the total energy of the system, which is decomposed, for convenience, into a site energy E_i and a bond energy V_{ij}. The indices i and j run over the atoms of the system, and r_{ij} is the distance between atom i and j. The function f_R and f_A represent repulsive and attractive part of the pair potential. The function f_c and b_{ij} are the cutoff function and bond-order function respectively.

Significant progress has been made in developing interatomic potentials for estimating the behavior of BN nanofillers with improved accuracy. For the modeling of BN nanofillers in MD based environment, most of the researchers have employed either Tersoff or modified form of Tersoff potential [21, 141-142]. Harmonic force field has also been employed by a couple of researchers for managing the atomic interactions in BN nanofillers [22, 143]. Tersoff potential that was initially introduced in paper [133] has been further modified by Brenner [144] to include additional terms for inherent over-binding of radicals and for non-local effects. In addition to Brenner [144], various researchers have also proposed optimized Tersoff potential

parameters for improving the accuracy of atomistic simulations. Sekkal et al. [145] proposed Tersoff parameters for boron by fitting the bulk properties of cubic BN. In their simulations, BN was treated as a single entity, hence, identical set of parameters were proposed for both boron and nitrogen. Tersoff potential parameters proposed by Sekkal et al. [145] are limited to BN interactions only, and cannot be extended to study interaction of boron or nitrogen with other atoms. These potential parameters [145] have been successfully employed by many researchers for predicting the structural and thermal properties of BN nanofillers. Sevik et al. [146] proposed parameters for Tersoff potential that effectively capture the experimental phonon dispersion in BN. Due to the capability of these parameters to effectively capture phonon dispersion, they are considered more suitable for estimating the lattice thermal conductivity of BN based nanostructures. Matsunaga et al. [147-149] proposed separate sets of parameters for boron, nitrogen and carbons atoms. This set of potential parameters is considered more suitable for reproducing experimentally measured lattice constants, bulk modulus and binding energy of cubic boron nitride. In addition to these parameters, Albe et al. [150-151] also proposed Tersoff potential parameters for bulk BN materials to simulate ion-beam deposition of BN thin films. One big advantage with parameters provided by Albe et al. [150-151] is that they account for the sp2 structure of BN bonding. The parameters proposed by Sekkal et al. [145], Sevik et al. [146], Matsunaga et al. [147-149] and by Albe et al. [150-151] have been summarized in **Table 1**.

Due to accurate parameterization that helps in achieving accurate fit with the DFT calculations and experimental results, Tersoff type potentials have generated more attention among the researchers for simulating the bonded interactions. On the other hand, reactive force field (ReaxFF) potentials are common among researcher for simulating the complex atomic structures of hydrocarbons [152-154]. In addition to hydrocarbons, ReaxFF has also been applied for BN

nanofillers and will be discussed further in next section. For ReaxFF potentials, parameters are obtained from fittings to the results of quantum chemical analysis. Similar to other empirical non-reactive potentials, the total energy of the system is derived from various partial energy contributions (bonded as well as non-bonded) as expressed in **Eq. (13)**.

$$E_{system} = E_{bond} + E_{over} + E_{under} + E_{val} + E_{pen} + E_{tors} + E_{conj} + E_{vdWaals} + E_{Columb} \quad \textbf{(13)}$$

Table 1. Compilation of parameters for Tersoff type potential proposed by different researchers.

Parameter	Sekkal et al.[145]	Sevik et al.[146]	Matsunaga et al. [147] (χ_{i-j}=1.1593)		Albe et al.[150]
	B-N	B-N	B-B	N-N	B-N
m	3.0	3.0	3.0	3.0	3.0
γ	1.0	1.0	1.0	1.0	1.0
λ3	0.0	0.0	0.0	0.0	1.9925
c	38049	25000	0.52629	79934	1092.9287
d	4.384	4.3484	0.001587	134.32	12.38
h	-0.57058	-0.89	0.5	-0.9973	−0.5413
n	0.72751	0.72751	3.9929	12.4498	0.364 53367
β	0.00000015724	0.0000001257	0.0000016	0.10562	0.000011134
λ2	2.22	2.199	1.5856	2.5115	2.784247207
B	346.7	340	183.49	219.45	3613.431337
R	1.95	1.95	1.95	2.15	2.0
D	0.2	0.05	0.15	0.15	0.1
λ1	3.468	3.568	1.9922	5.7708	2.998355817
A	1393.6	1380	277.02	11000	4460.833973

ReaxFF type potentials are reported to be more suitable for simulating bond-breaking and bond-forming mechanisms. Fundamental difference between ReaxFF and most of the other empirical interatomic potentials is that ReaxFF does not employ any fixed connectivity for the bonded interaction. In ReaxFF type potentials the bond order is directly calculated from the instantaneous interatomic distance r_{ij}, which keeps on updating during the simulation. This bond order is responsible for creation and dissociation of bonds during the simulation. The mathematical expression for calculating the bond order with respective details can be found in the papers [152-154].

In MD based simulations, strain calculations are performed with the help of initial (Li) and final (L_f) lengths of the simulation box as expressed by **Eq. (14)**. The concept of stress in a material or a body is well known at the continuum level and usually referred as Cauchy stress tensor. However, at atomistic level the principles of continuum are not applicable, and hence an alternative stress referred as virial stress is estimated at atomistic level. The virial stress is the most commonly used definition of stress in discrete particle systems. Virial stress is the summation of two components. The first component depends upon the mass and velocity of the atoms in the MD simulations, whereas the second component depends upon the interatomic forces and atomic positions. The mathematical expression for virial stress as the summation of two components is given by **Eq. (15)**.

$$\epsilon = \frac{L_f - L_i}{L_i} \tag{14}$$

$$\sigma_{ij}^{\alpha} = \frac{1}{\varphi^{\alpha}}\left(\frac{1}{2}m^{\alpha}v_i^{\alpha}v_j^{\alpha} + \sum_{\beta=1,n} r_{\alpha\beta}^{j} f_{\alpha\beta}^{i}\right) \tag{15}$$

Where *i* and *j* denote indices in Cartesian coordinate system; α and β are the atomic indices; m^{α} and v^{α} are mass and velocity of atom α; $r_{\alpha\beta}$ is the distance between atoms α and β; and φ^{α} is the atomic volume of atom α.

The strain energy based concepts, as discussed in DFT section, are also applicable in MD simulations for estimating Young's modulus and 2D Young's moduli values of the system as per **Eq. (5), (6)** and **(7)**. In addition to predicting the mechanical behavior of an atomistic system, the MD based simulations have also been employed for predicting the thermal behavior of the system. Thermal conductivity (*k*) of a simulated atomistic configuration can be estimated by using the mathematical expressions given below:

$$k = \frac{J}{2A\left(\frac{\partial T}{\partial x}\right)} \quad \textbf{(16)}$$

$$J = \frac{\sum 0.5 N_{transfer}(m_h v_h^2 - m_c v_c^2)}{t_{transfer}} \quad \textbf{(17)}$$

Here, in **Eq. (16)** and **(17)**, $\frac{\partial T}{\partial x}$ refers to the temperature gradient along the direction of heat flux (*J*), *A* is the cross sectional area, *h* and *c* refer to the hot and cold atoms, $N_{transfer}$ and $t_{trasfer}$ are summation time and number of exchange respectively.

3.0 MD based simulations for BN nanofillers

As described in previous sections that atomistic modeling techniques are emerging as a potential tool to predict the mechanical and thermal behavior of BN nanofillers. MD based simulations are considered sufficiently accurate and less computational intensive as compared to FEM and

DFT based approaches, respectively. In this part of the article, authors have made an attempt to review the current state of art in simulating the mechanical as well as thermal behavior of BN nanofillers with the help of molecular dynamics.

Mechanical behavior:

Mechanical behavior of BN nanofillers has been widely investigated by many researchers. Among various mechanical properties, Young's modulus is considered as the most widely predicted or estimated property of any material. Mechanical properties of BN nanofillers (BNNS or BNNT) predicted or estimated by using different means have been compiled in table 2 and table 3. It can be inferred from these tables that researchers have simulated BN nanofillers both as an isotropic as well as in-plane orthotropic material (arm-chair and zig-zag configuration). While treating BNNS as an isotropic material [18-20, 75, 100, 106, 109, 111, 155-157], researchers have predicted a range of Young's modulus starting from 0.79TPa to 0.97TPa (assuming 0.33 nm as the thickness of a BNNS). Similarly, for BNNTs, the Young's modulus values with isotropic material properties range from 0.77TPa to 1.2TPa [16, 23-24, 109, 142, 158]. In addition to Young's modulus, researchers have also predicted the 2D Young's modulus for BN nanofillers as tabulated in table 3. At the atomistic level, these nanofillers are not isotropic in nature and usually have in-plane orthotropic properties that are dependent on the chirality vector. Based on the alignment of the bonds with the loading direction, BN nanofillers (BNNT or BNNS) can be further classified as zig-zag and armchair configurations. Young's modulus (Y) as well as 2D Young's modulus (Y_S) for zig-zag and armchair directions have also been summarized in in table 2 and table 3, respectively [17, 21-22, 26, 124,126, 143, 159-161]. It can be inferred from these tables that 2D Young' modulus (Y_S) predicted through atomistic simulations and experimental techniques lies in the range of 200N/m to 500N/m [75].

Le [21] performed MD simulations using Tersoff- potential parameters provided by Sevik et al. [146] to predict mechanical properties of BNNSs. In this study, author extended the small cut-off distance to large cut-off distance and obtained lower values of fracture stress and strains as compared with earlier studies [159]. Fracture strain predicted by Le [21] was in good agreement with DFT calculations performed by Topsakal et al. [126]. Molecular dynamics based simulations has been performed by Verma et al. [26] to estimate the Young's modulus and shear modulus of BN nanofillers. In their computational work, interatomic interactions between boron and nitrogen atoms were estimated with the help of Tersoff-type potentials [134-135] with parameters obtained from the work of Sekkal et al. [145]. The potential parameters provided by Sekkal et al. [145] were slightly modified by Verma et al. to obtain best fit for bond length and cohesive energy of h-BN sheet. Verma et al. [26] predicted the values of Young's modulus for BNNT as 1.11TPa and 0.98TPa in armchair and zig-zag directions respectively. Nearly same values of Young's modulus were predicted for BNNSs i.e. 1.11 TPa and 1.0 TPa in arm-chair and zig-zag directions, respectively. They further validated their computational model with the help of experimental results reported in the work of Chopra et al. [23]. It was concluded in the research work of Verma et al. [26] that the Young's modulus of small diameter BNNTs increases with increase in diameter and attains maximum value of 1.11TPa at the radius of 0.95 nm, and then falls with further increase in diameter as illustrated in **Fig. 5**(left). On the other hand, shear modulus decreases with increase in diameter of the BNNT and attains a constant value at higher tube diameter as shown in **Fig. 5** (right).

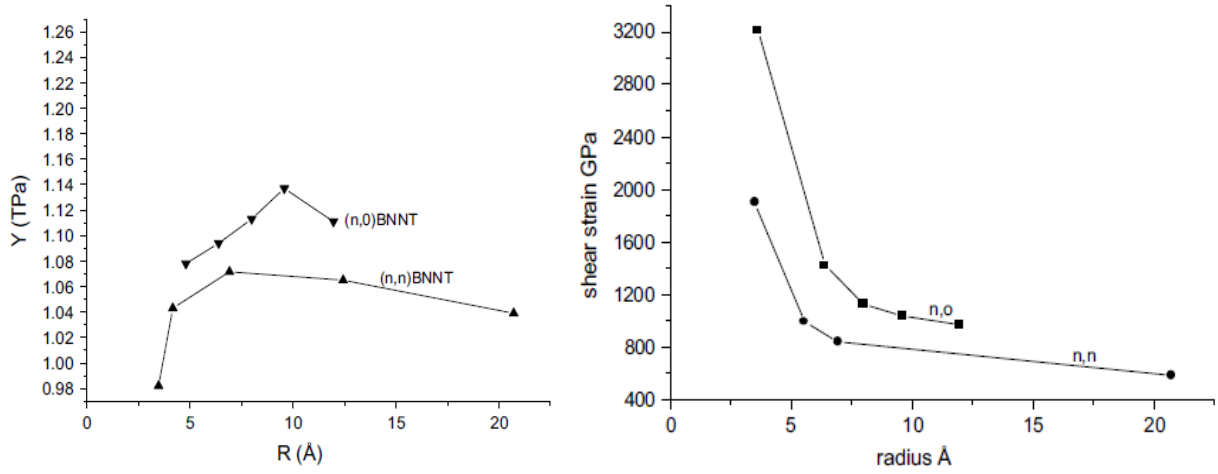

Fig. 5. Variation of Young's modulus (left figure) and shear strain (right) with respect to radius of BNNT (Reproduced with permission from [26])

Zhang et al. [142] studied intrinsic twisting of helical BNNTs with the help of tight-binding MD method [TBMD], and estimated Young's and shear modulus values, as 0.850 and 0.370 TPa, respectively. In 2012, Mortazavia and his research team [159] performed MD based simulations to study the tensile behavior of BNNSs. In their computational work, Tersoff potential was used in conjunction with optimized parameters obtained from the work of Matsunaga et al. [147,149]. It was predicted in their computational work that BN nanostructures failed in a brittle manner, and had Young's modulus in the range of 0.8-0.85 TPa.

MD based studies [162-163] have also been performed to investigate the effect of grafted carboxyl group on the elastic properties of BNNTs. Yuan and Liew [162] studied the effects of grafting carboxyl groups on the elastic properties of BNNTs. It was predicted in their computational work that Young's moduli of nanotubes started deteriorating with the attachment of carboxyl group. The zig-zag configuration of BNNTs was reported to be affected most as compared to the armchair configuration.

Table 2. Mechanical properties of BN nanofillers from different studies with different methods.

Method	Reference	Nanofiller	Young's Modulus (TPa)	Fracture Stress (GPa)	Fracture Strain (%)	Poisson's Ratio
Experimental	Chopra et al. [23]	BNNT	1.22 ± 0.24	-	-	-
	Suryavanshi et al. [24]	BNNT	0.722	-	-	-
	Wei et al. [158]	BNNT	0.895	33	3	-
	Arenal et al. [16]	BNNT	1.11 ± 0.17	-	-	-
	Bosak et al. [100]	BNNS	0.811	-	-	-
DFT	Hernández et al. [124]	BNNT	0.884 ZZ 0.912 AC	-	-	0.23-0.27
	Fakhrabad et al. [25]	BNNT	0.821 AC 0.764 AC	-	-	-
	Ohba et al. [155]	BNNS	0.952	-	-	-
	Mirnezhad et al. [156]	BNNS	0.829	-	-	0.21
	Zhang et al. [142]	BNNT	0.850			
MD	Verma et al. [26]	BNNT	0.982 ZZ 1.111 AC	-	-	0.13 ZZ 0.16 AC
		BNNS	1.004 ZZ 1.111 AC	-	-	-
	Mortazavi et al. [159]	BNNS	0.800 ZZ 0.850 AC	165	30	-
	Zhao et al. [152]	BNNS	0.693 ZZ 0.740 AC	120	28	-
	Han et al. [157]	BNNS	0.881	133	33	-
Structural Mechanics & Others	Eun-Suok Oh [109]	BNNS BNNT	0.977 0.950	-	-	0.17
	Boldrin et al. [106]	BNNS	0.797	-	-	0.21
	Green et al. [111]	BNNS	0.803	-	-	-

Table 3. Mechanical properties of BN nanofillers from different studies with different methods

Method	Reference	Nanofiller	Young's Modulus (N/m)	Fracture Stress (N/m)	Fracture Strain (%)	Poisson's Ratio
Experimental	Li et al. [75]	BNNS	200-500	-	22	-
DFT	Kudin et al. [17]	BNNT	266 ZZ 267 AC	-	-	0.21
	Sahin et al. [18]	BNNS	267	-	-	0.21
	Topsakal et al. [126]	BNNS	258 AC	-	-	-
	Andrew et al. [19]	BNNS	276	-	-	0.22
	Peng et al. [20]	BNNS	278	-	-	-
MD	Minh-Quy Le [21]	BNNS	263 ZZ 253 AC	36 ZZ 30 AC	23 ZZ 17 AC	-
	Minh-Quy Le [22]	BNNS BNNT	284 AC& ZZ 283 AC& ZZ	-	-	-
	Minh-Quy Le [143]	BNNS	296 ZZ 286 AC	-	-	-
	Le and Nguyen [161]	BNNS	258 ZZ 251 AC 257 ZZ 249 AC 257 ZZ 251 AC 258 ZZ 251 AC	38 ZZ 36 AC 31 ZZ 30 AC 35 ZZ 32 AC 31 ZZ 33 AC	26 ZZ 26 AC 17 ZZ 18 AC 21 ZZ 20 AC 17 ZZ 22 AC	- - - -
Structural Mechanics	Minh-Quy Le [143]	BNNS	332	-	-	-

It was further concluded in the research of Yuan and Liew [162] that the reduction in elastic modulus for zig-zag direction was least affected by the quantity of attached carboxyl group, whereas the reduction in armchair direction depends on the quantity of the chemical group. Recently in 2014, Ghazizadeh et al. [163] conducted a MD based study on the mechanical properties of hydrogenated BNNTs. MD simulations were performed in conjunction with the Universal force field (UFF) and Dreiding potentials [164-166]. It was concluded in their research that the Young's modulus of BNNTs showed a decreasing trend when hydrogen atoms were bonded with all available nitrogen atoms.

Buckling behavior:

In 2001, Srivastava et al. [166] investigated the stiffness and plasticity of BNNTs. They studied the implications of rotated BN bonds on the buckling behavior of zig-zag nanotubes, and reported anisotropic strain release followed by anisotropic plastic buckling for axially compressed BNNTs. In their research paper [166], they also proposed a ''skin-effect'' model for smart nano composite materials that can localize structural damage towards the skin or surface side of the material. Nejad et al. **[**167**]** also investigated the buckling behavior of open-ended boron nitride nanotubes. They performed MD based simulations with the help of optimized Tersoff potential parameters obtained from the work of Liao et al. [168]. In their conclusion, it was reported that hydrogen physisorption decreased the buckling stability of BNNT by 10% in the temperature range of 300-3000°K as compared to pristine BNNTs. Hai-jun Shen [169] performed MD based simulations to compare the effect of radial compression on BNNT and CNT. The author predicted a comparable radial compressive stiffness for both CNTs and BNNTs. However, it was also observed in their simulations that BNNT had lower energy absorbing, load-support and deformation-support capabilities as compared to CNT. Nejad et al.

[170] examined the behavior of fixed length BNNTs with varying diameters. MD simulations were performed with the help of Lennard-Jones [137] and harmonic potentials. It was concluded in their numerical simulations that critical buckling loads exhibited an increasing trend with an increase in nanotube diameter.

Slotman and Fasolino [171] compared the bending rigidity of BNNTs with that of graphene. Simulations were performed with the help of Tersoff potential [136] in combination with optimized parameters obtained from the work of Albe et al. [151]. It was also predicted in their computational model that BNNSs had lower bending rigidity as compared to that of graphene sheets. In 2010, Liao et al. [172] investigated the effects of temperature on the tensile and compressive behavior of BNNTs. They performed MD simulations in conjunction with the Tersoff potential parameters proposed by themselves after fitting MD simulation results to the one obtained from density functional theory. These potential parameters were suggested to be more suitable for the simulation of nano-sized BNNTs and also for simulating their bond breaking behavior. It was reported in their work that both failure as well as buckling strain got decreased with increase in temperature. It was further noted from their computational model that BNNTs failed in a chain like mode without any obvious yielding in tension, as shown in **Fig. 6** whereas no chain formation was observed under compressive loading. Shokuhfar and his team [173] investigated the effect of temperature (up to 3000^0 K) on the buckling behavior of BNNTs using potential parameters provided by Albe et al. [151]. It was predicted in their computational model that higher modeling temperatures reduced the value of critical buckling load as well as in critical buckling strain. Similar kind of study on BNNSs was performed by Yuan and Liew [174]. They performed their investigation with the help of MD simulations in conjunction with

universal force field UFF [164]. A higher value of buckling strain was predicted in the MD simulations for zig-zag configuration of BN nanofillers as compared to armchair.

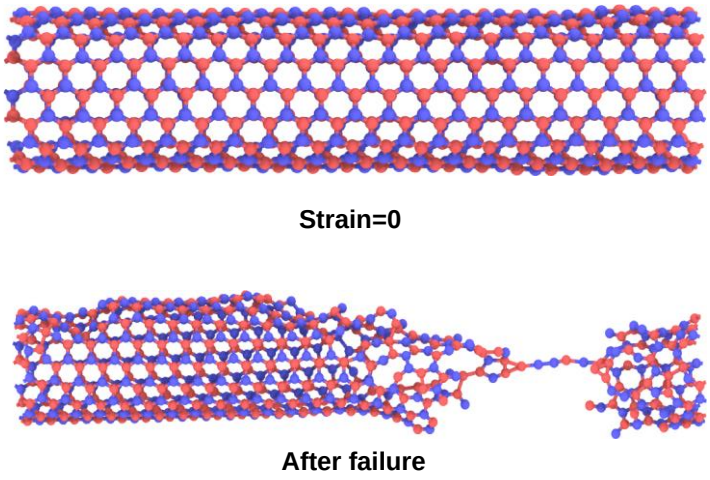

Fig. 6. Deformation morphology of a BNNT subjected to tensile loading with chain (Adapted from [172], Simulations, with similar conditions as in [172], were performed by authors of this paper to reproduce this image)

Defects in BN nanofillers:

BN nanofillers prepared experimentally are not flawless and usually contain some native defects such as vacancies, dislocation, Stone wales defects etc. Existence of defects in BN nanofillers has already been established by experimental as well as theoretical studies [175-176]. The following section reviews MD based studies conducted on defective BN nanofillers and effects of these defects on their mechanical and thermal properties.

Griebel et al. [177] used MD based simulations in conjunction with Parrinello-Rahman [178] approach to study the impact of vacancy defects and functionalization on the Young's modulus of BNNTs. In their numerical work, Tersoff potential in conjunction with parameters provided by Matsunaga et al. [147] was used to estimate interactions between boron and nitrogen. In the

original parameters proposed by Matsunaga et al. [147] the possibility of bond formation between same atoms was excluded by only accounting for repulsive forces. But in the work of Griebel et al. [177] the potential parameters were adapted to deal with B-B and N-N bonds as well. In order to account for homo- elemental bonds formation attraction term was also included in the potential function.

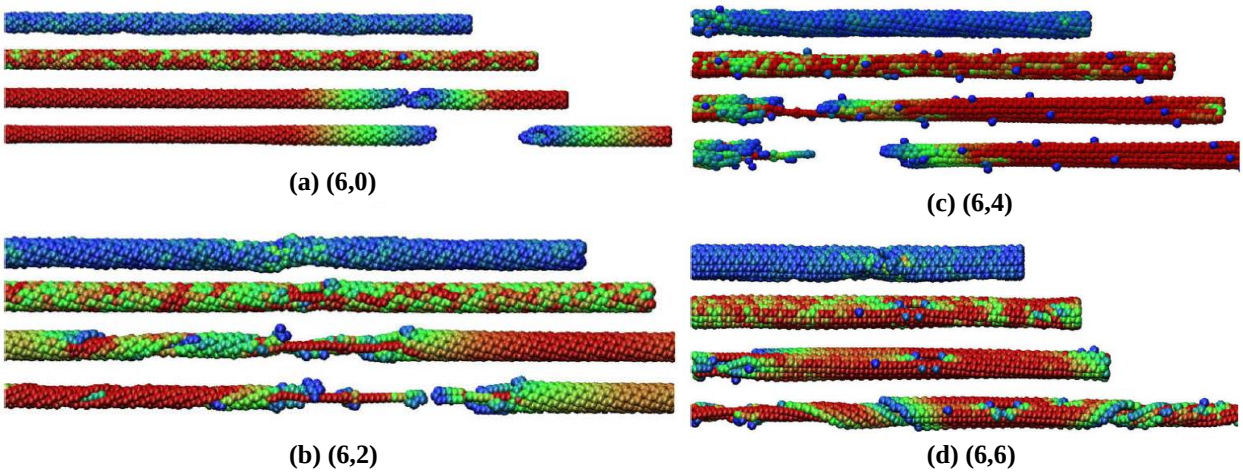

Fig. 7. Stress induced deformation and failure of BNNT with different chirality. Colors scheme refers to level of stress per atom values from blue over green to red. Four snapshots for each chiral nanotubes refers to, no strain, strain before, at and after failure states. (Reproduced with permission from [177]).

In their work, it was predicted that the Young's modulus of BNNTs starts detereorating with an increase in concentration of vacancy defects. This reduction in Young's modulus was found to be independent of the tube-chirality. In order to better visualize the mode of failure with single defect in BN nanotubes with different chirality, snapshots from the simulation box at different level of strain have been shown in **Fig. 7**. Griebel and his team [177] also investigated the effect

of functionalization on the Young's modulus of BNNTs, and summarized the effect of functionalization as shown in **Fig 8**. A general decrease in the value of Young's modulus up to 2/3 of pristine BNNT can be inferred from the plotted data in **Fig. 8**. No significant effect of functionalizing was observed in the range of 60% to full functionalization for zig-zag configuration, whereas a slight increase in Young's modulus was reported for armchair configuration between the same ranges of functionalization.

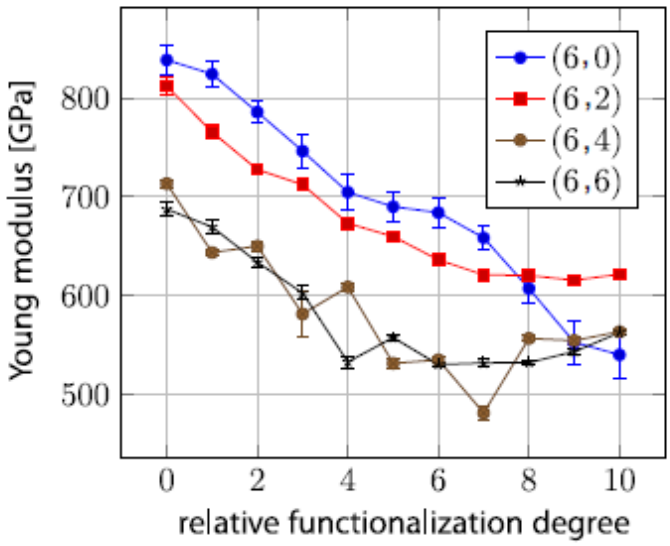

Fig. 8. Young's modulus estimated as a function of relative functionalization degree for (6, m) BN nanotubes (Reproduced with permission from [177]).

Shokuhfar et al. [179] carried out MD simulations with GROMACS harmonic potential parameters for bonded interactions. In their MD based simulations the harmonic potential parameters were obtained by fitting the potential parameters of Liao et al. [168] to the DFT calculations. In their simulations, NVT ensemble was enforced to study the effect of vacancy on the critical buckling performance of BNNTs, and it was reported in the conclusion that the B–N-double vacancy was most detrimental to the structural strength, followed by B-vacancy and N-vacancy defects. It was also reported in their work that B-type vacancy was most detrimental to

the fracture strain. In order to visualize the failure modes under compressive loading, snapshots from the simulations for BNNTs at the time of failure have been shown in **Fig. 9**. It can be inferred from the snapshots that the failure morphology of BNNTs are chirality dependent.

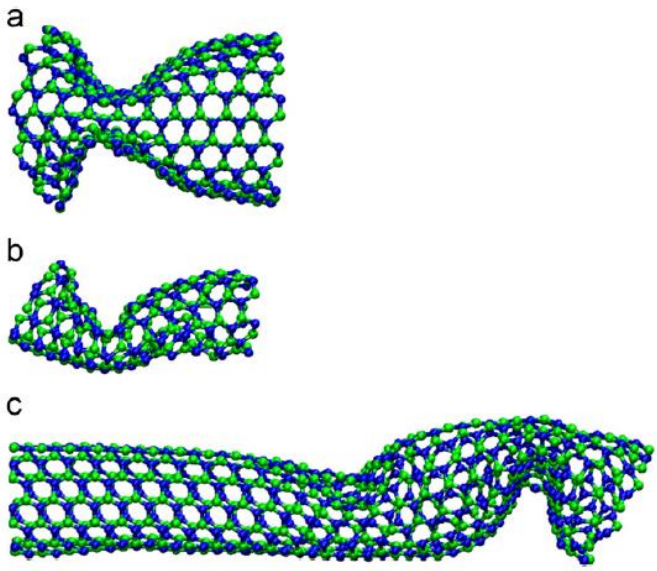

Fig. 9. Defective BNNT after compressive buckling (a) (10, 10) (b) (5, 5) (c) (7, 7) (Reproduced with permission from [179])

Le and Nguyen [161] examined the effect of vacancies and stone-wales (SW) defects on the tensile properties of h-BN nanosheets. Tersoff potential in conjunction with parameters obtained from Sevik et al. [146] was employed to simulate atomistic interactions. In order to avoid the overestimation of maximum force to break the bond the cutoff function was removed from the potential function ($f_c(r_{ij})$=1). Notion that overestimation of maximum forces can be avoided by removing cutoff function has been proposed by the author with the help of **Fig. 10**. It can be inferred from their plotted data in **Fig. 10** that potential energy and force reduce smoothly to zero as bond strain increases with removed cutoff function. Le and Nguyen [161] employed finite

element in conjunction with the MD based simulations. The relaxed atomic positions of B and N atoms were determined with the help of MD simulations. It was concluded in their computational model that a centrally located single-defect noticeably reduced the fracture stress and strain values, as compared to those of pristine sheets. Young's modulus of BNNSs was reported to be unaffected due to the presence of single vacancy but di-vacancy had detrimental effect on the values of fracture stress and strain. It was further observed that reduction in fracture properties was dependent on applied loading direction and orientation of Stone–Wales defects.

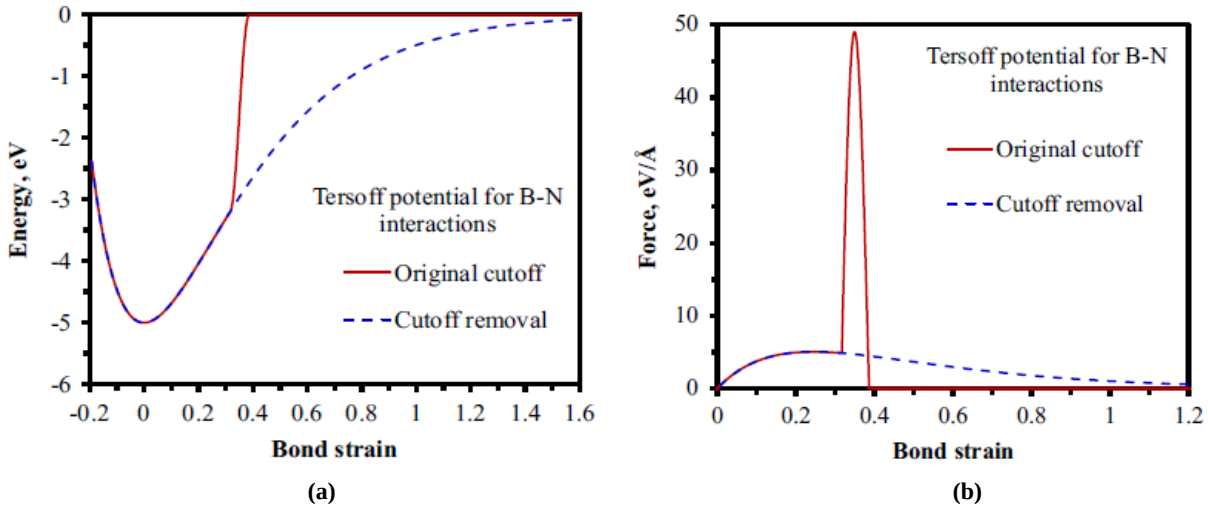

Fig. 10. (a) Potential energy vs bond strain (b) Force vs bond strain, with keeping bond angle value constant according to Tersoff potential (reproduced with permission from [161])

Recently in 2014, Sarma and his team [180] used the MD based simulations in conjunction with reactive force fields potentials (ReaxFF) with parameters taken from the work of Weismiller et al. [153]. It was predicted in their simulations that the point and line defects significantly reduced the tensile strength of BNNTs. Tube diameter and simulation temperature also had a significant effect on the tensile behavior of BNNTs. Similar to the work of Sarma et al. [180], MD based simulations with Tersoff-Brenner potential [144] were also performed by Krishnan et al. [181] to

investigate the effects of vacancy and Stone-Wales (SW) defects on the failure behavior of BNNTs. The simulations were performed with the help of potential parameters proposed by Sevik et al. [146]. It was concluded in their work [180] that BNNTs in armchair configuration were highly sensitive to defects, whereas the zig-zag configurations were the least sensitive.

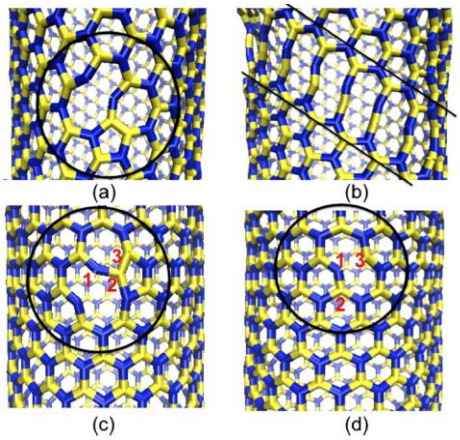

Fig. 11. (a) Breaking of B-B bond in 5-7-7-5 defect in arm chair configuration (b) Formation of decagon with the propagation of bond breaking (c) Breaking of B-B bond in zig-zag configuration (d) Rotation of defective B-N bonds to regain the pristine form (Reproduced with permission from [181])

Pristine nanotubes (both armchair as well as zig-zag) failed in brittle manner whereas in case of defective nanotubes only the zig-zag configuration of nanotubes underwent brittle failure. The defect-induced plastic behavior was also observed in armchair BNNTs. Activation of different failure mechanisms in zig-zag and arm-chair configurations of BNNTs resulted in plastic failure for armchair configuration and brittle failure for zig-zag configuration. In armchair configuration of BNNT, once the bond in pentagon breaks it leads to failure of bonds oriented at an angle of 30° to the axis of BNNT as shown in **Fig. 11(a)**. This failure of bonds aligned at an angle leads to the formation decagons-chain, as shown in **Fig. 11(b)**. This sequence of events in armchair

configuration induces plastic behavior in BNNTs. This plastic behavior due SW defects had a strong radius-dependency in the armchair configuration of BNNTs, and turned to brittle behavior with radii greater than 2.5 nm as in case of (20, 20) BNNT. In case of zig-zag configuration of BNNT, formation of decagon due to failure of B-B bond is followed by the failure of N-N bond which in turn is followed by the failure of N-N bond and then rotation of bond between B-N. This bond rotation further resulted in formation of two new B-N bonds. The formation of these two new bonds brought back the pristine form and resulted in a brittle failure as compared to armchair configuration.

Mortazavi and Cuniberti (2014) [182] examined the properties of polycrystalline BN nanosheets using Tersoff-potential [134] in conjunction with optimized parameters proposed by Matsunaga et al. [149]. They concluded in their work that a reduction in grain size ultimately resulted into a gradual decrease in elastic moduli of polycrystalline films. They also suggested that experimentally fabricated polycrystalline BN nanosheets might possess remarkably high mechanical properties. Moon and Hwang [183] performed MD based simulations using Tersoff potential [133-136] in combination with parameters proposed by Albe et al. [150-151] to examine the structural and thermal behavior of BNNTs. It was reported in their computational work that strain energy had a decreasing trend with an increase in nanotube diameter. The strain energy found to be proportional to the inverse of square of tube diameter. At higher temperature, Stone-wales SW defects were found in nanotubes during their thermal treatment. Also the formation energy of SW defects increased with an increase in diameter of the nanotubes.

Failure/fracture:

In addition to the elastic properties of BN nanofillers, their fracture behavior has also been investigated by many researchers with the help of MD based platform. In 2011, Liao et al. [168] investigated the deformation of armchair BNNTs under subjected to axial tensile strains using a modified version of Tersoff potential parameters developed by Albe et al. [150]. The modified set of parameters predicted a better bond breaking behavior. A chain like failure mode (as discussed and explained earlier w.r.t to ref. [172]), without any noticeable yielding, was reported in their computational work. Wei et al. [184] examined and compared the behavior of CNTs and BNNTs subjected to tensile as well as compressive loading. In their atomistic simulation, it was concluded that under compression, zig-zag configuration of CNTs as well as BNNTs had higher Young's modulus as compared to armchair configuration of respective nanotubes. It was also concluded from the computational model of Wei et al. [184] that fracture behavior of CNTs or BNNTs is dependent on the chirality, and the nanotubes with the same chirality had similar deformation patterns regardless of material.

Tian et al. [185] investigated the impact of shear displacement on the mechanical properties, wrinkling patterns and fracture behavior of h-BN nanosheets. In order to study the wrinkling in a single BN nanosheet, an analytical model was developed with geometrical parameters and boundary conditions as shown in **Fig. 12**. In **Fig. 12**, L, H and t are length, width and thickness of the plane, respectively, E and ν are Young's modulus and Poisson's ratio, respectively. The schematic of one wrinkle in a nanosheet is shown in **Fig. 12**, where σ_ξ and σ_η are the applied stresses in ξ and η directions respectively. The mathematical expressions for shear stresses σ_ξ and σ_η have been provided in **Eq. 19**, where γ is referred as δ/H.

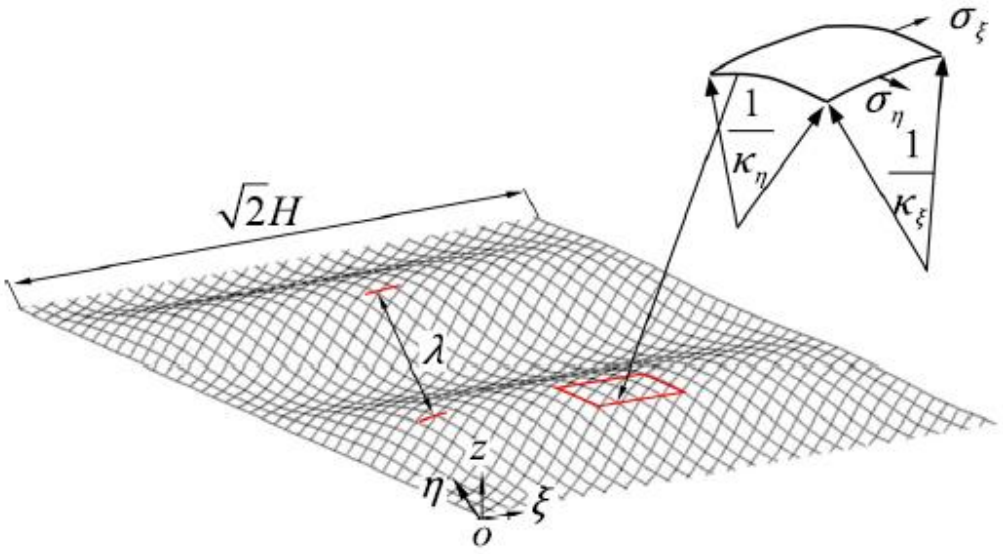

Fig. 12. Single wrinkle in a nanosheets (Reproduced with permission from [185])

The out of plane displacement ω with respect to mode shape is given mathematically by **Eq. (18)**. In this **Eq. (18),** A and λ refer to the amplitude and wavelength of the wrinkle.

$$\omega = A \sin\frac{\pi\xi}{\sqrt{2H}} \sin\frac{2\pi\eta}{\lambda} \quad \textbf{(18)}$$

$$\sigma_\eta = -\frac{\pi^2 E t^2}{3(1-\nu^2)\lambda^2} \quad \textbf{(19.a)}$$

$$\sigma_\xi = E\frac{\gamma}{2} \quad \textbf{(19.b)}$$

$$\sigma_\eta \kappa_\eta + \sigma_\xi \kappa_\xi = 0 \quad \textbf{(20)}$$

In the analytical model proposed by Tian et al. [185] the stress state equilibrium equation is established as **Eq. (20)**, where κ_η and κ_ξ are the curvatures along the direction η and ξ, respectively.

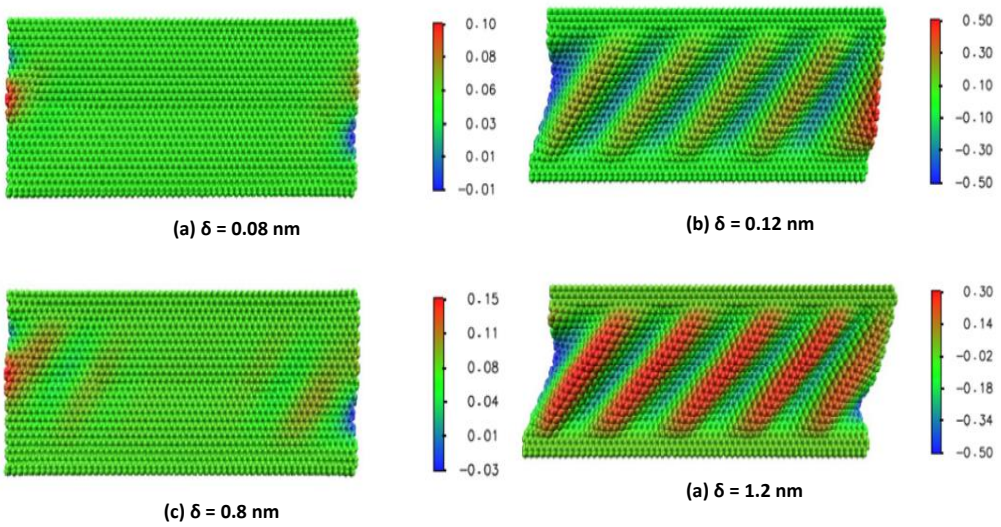

Fig. 13. Wrinkling pattern of nanosheets with respect to shear displacement δ (Reproduced with permission from [185])

It can be inferred from the wrinkling pattern of monolayer BNNS, shown in **Fig. 13(a),** that wrinkling initiates at a point when in-plane shear displacement (δ) reaches critical buckling value of 0.08 nm. At critical buckling the wrinkle initiates from the free edges and keeps central part of sheet wrinkle-free. Further increase in shear displacement results in a uniform distribution of wrinkle patterns with identical crest and trough as indicated in **Fig. 13(c)**. It can be inferred from the results obtained from the simulations of Tian et al. [185] that average wrinkling amplitude of the nanosheets increases with increase in shear displacement, whereas the wrinkling wavelength has a reverse effect as indicated in **Fig. 14(a) and Fig. 14(b),** respectively.

An important contribution regarding MD based simulations on boron nitride came from Han et al. [157], who studied the effects of temperature, strain rate and crystal orientations on the mechanical properties of BNNSs. The interaction between boron and nitrogen atoms were described by the parameters proposed by Albe et al. [150-151]. It was observed that the nanosheets were basically an anisotropic material and any increase in the temperature led to a

decrease in Young's modulus, fracture strength and fracture strain. A reduction in Young's modulus was observed with an increase in strain rate, while reverse effect was observed on fracture strength of BNNSs. Perim et al. [186] appraised the fracture behavior of defective carbon and boron nitride nanotubes in accordance with MD based simulations in conjunction with ReaxFF force field [152-154]. The similarities and differences in their (CNT and BNNT) fracture patterns were outlined, under similar stress conditions.

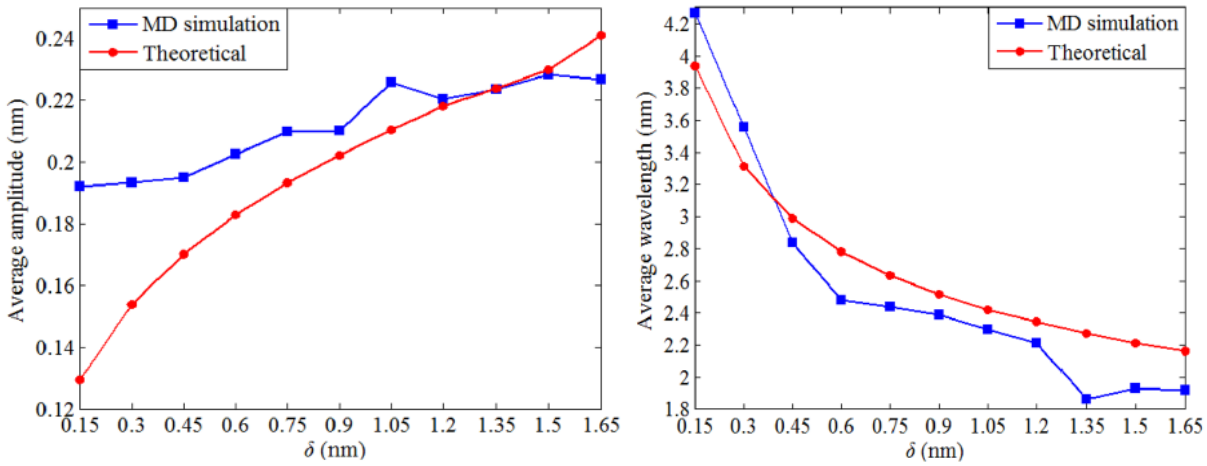

Fig. 14. Influence of shear displacement on wrinkle profile. (Reproduced with permission from [185])

Chirality & torsion:

Krishnan and Ghosh [187] studied the effect of chirality on the elastic properties of single-walled BNNTs subjected to tensile and torsional loading. Their simulations were performed with the help of Tersoff-potential parameter set provided by Sevik et al. [146]. They concluded in their simulation results (as shown in **Fig. 15**) that with an increase in aspect ratios (lengths to diameter ratio of a nanotube) elastic modulus also increases. It can also be inferred from their summarized data in **Fig. 15** that at higher aspect ratios variation in Young's modulus is comparatively small.

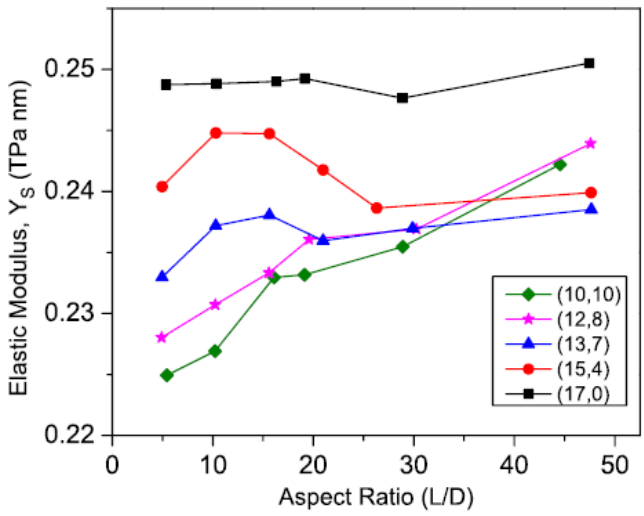

Fig. 15. Elastic modulus of BNNT with respect to aspect ratio (Reproduced with permission from [187])

Recently in 2014, Ansari and Ajori [188] studied the torsional vibration performance of double-wall BNNTs using Tersoff-potential parameters developed by Albe et al. [150]. They extended MD simulations in conjunction with continuum modeling to estimate shear modulus of nanotubes. Torsional frequency was predicted to be varying with geometrical parameters such as length and boundary conditions. Moreover, torsional frequency of BNNTs was observed to be higher than that of their carbon counterparts i.e. nanotubes (CNT).

Ajori and Ansari [189] employed MD based simulations with Tersoff-like potential and parameters reported by Albe and Moller [150] to investigate the torsional buckling response of BN nanotubes. In their simulations, (6, 6) and (10, 10) armchair BNNTs with length varying from 5.13 nm and 15.4 nm were opted for investigation. They predicted size dependent values of shear modulus which differed from 0.64TPa at 5.13 nm and finally converging to a value of 0.75TPa as the tube length was increased. Critical torque was found to be highly dependent upon

the geometrical parameters such as length, chirality and boundary conditions. The critical shear strain was predicted to be independent of chirality.

Minh-Quy Le [190] investigated the dependency of mechanical properties of BN nanoribbons on their size using potential parameters for boron and nitrogen from the work of Sevik et al. [146]. In case of rectangular nanoribbons, tensile properties were found to be significantly affected by the length to width ratios. While size effects were found to be low in case of square boron nitride nanosheets as compared to that of rectangular ones. It was also observed that Young's modulus, fracture stress and fracture strain had an increasing trend with decreasing width for zigzag configuration of nanoribbons with fixed length. In case of armchair BN nanoribbons with constant length these properties varied slightly as compared to zig-zag configuration. BN nanoribbons showed higher mechanical strength in zigzag direction as compared to armchair direction. Tang et al. [191] investigated the effect of interfacial-structure on the mechanical properties of BN nano-bamboos (BNNB) [192-193]. In these simulations, interaction between boron and nitrogen atoms were modeled by Tersoff-like potential [134] with parameters taken from the work of Albe et al. [151], and the van der Waals interactions at interfaces were modeled with the help of Lennard-Jones (LJ) potential [137]. BNNBs with interlocked joint interfacial structures with compressive interfacial stresses, showed higher tensile fracture strength and Young's modulus up to 8.0GPa and 225GPa, respectively. Due to these interlocked joint interfacial structures a shift from an inter-planar sliding mode to an in-plane tensile elongation mode was observed in the deformation mechanism.

Thermal conductivity:

BN nanofillers have exceptionally high thermal conductivities. Molecular dynamics based simulations have the capability to accurately predict the thermal conductivity of these nanofillers under different type of boundary and loading scenarios. Shen [194] studied the variation in thermal conductivity of BNNTs with temperature and tube diameter with the help of Tersoff type potentials parameters proposed by Albe et al. [150]. It was observed in his computational work that the thermal conductivity had a decreasing trend with an increase in the temperature and tube diameter. Sevik et al. [146] studied the thermal transport properties of BN nanostructures using parameterized Tersoff-potential under (NVE) micro-canonical ensemble. Though, BN nanostructures were found to be possessing quite high thermal conductivities, but lower as compared to their carbon counterparts. But qualitatively, both carbon and BN nanoribbons showed similar behavior with respect to the variation in width and edge structure (zig-zag and armchair). It was further concluded that thermal conductivities were independent of chirality. Mortazavi and Rémond [159] also evaluated the thermal conductivity of a single-layer of BN nanosheet through MD simulations with parameters for boron and nitrogen taken from the work of Matsunaga et al. [147-149] and predicted a value of 80W/m-K for thermal conductivity of the nanosheet.

Kinaci et al. [195] investigated the variation in thermal conductivity (κ) of hybrid graphene/h-BN nanostructures with stripe super-lattices (alternate stripes of graphene and BN) and BN dots embedded in graphene. The parameters for boron, nitrogen and carbon interactions were developed by the author and his team using B-N parameters from Sevik et al. [146] and carbon interactions from the work of Lindsay and Broido [196]. For stripe super-lattices, it was predicted that interface in zigzag configuration produced a higher κ in the direction parallel to the interface than the armchair configuration, while the perpendicular conductivity was less

prone to the details of the interface and was limited by the thermal conductivity of h-BN. However, the embedded dot structures having mixed zigzag and armchair interfaces, had a strong effect on the thermal transport properties than super-lattices. Recently in 2014, Chen et al. [197] examined the thermal conductivity of BN nanoribbons in various transport directions (from 0^0 to full 30^0 chirality) using non-equilibrium molecular dynamics based simulations with the use of Müller-Plathe [198] method and Tersoff-type three-body potential [195]. Edge specularity for the boundary scattering (which is closely related to the edge roughness) was also studied with respect to different chiral angles. It was concluded that both thermal conductivities and edge specularity attained local maxima at chiral angel of 19.11^0. Thermal conductivity predicted to be increasing with an increase in the ribbon length up to a certain critical length value depending upon the chiral angle.

Sevik et al. [199] investigated the effect of boron isotopes on the thermal conductivity of BN nanotubes. It was concluded that thermal conductivity varied in the range of 450–500 W/m^{-1} $K^{-1}$and 340–400 W/m^{-1} $K^{-1}$for isotopically pure (100% 11B) and natural (80% 11B) BNNTs and h-BN nanosheets, respectively. In addition to these quantitative results, a temperature dependency of thermal conductivity of BNNT's on isotopes was also studied with the same computational model. It was also concluded from their atomistic model that effects of isotopes were more significant at the lower temperatures. Scattering of phonon from isotopes at lower temperatures was associated with the reduction in thermal transport phenomenon. Sevik et al. [199] further concluded that the effect of isotopes was more pronounced in 3D structures as compared to 1D and 2D structures. This dependency of thermal conductivity on structures was considered to be associated with average isotope-isotope separation, where smaller distances reduced the relaxation length, ultimately reducing the lattice thermal conductivity. Haijun Shen

[200] examined and compared the thermal conductivities of CNTs and BNNTs, under radial compression, with the help of Tersoff-potential [135]. It was predicted in his work that under local as well global compression, the thermal conductivity exhibited a decreasing trend. But global compression had a more profound effect than local compression. In addition to that an increase in temperature resulted into the lowering of thermal conductivity. Mashreghi [201] also conducted a MD based study on thermal expansion/contraction of armchair BNNTs in various directions i.e. axial, radial and circumferential. Boron and nitrogen interactions were modeled using parameters provided by Albe et al. [150]. Coefficients of thermal expansion (CTE) were estimated along the axial direction with different diameters. The CTE in radial direction was reported to be lower as compared to circumferential direction.

Hybrids:

So far, this review paper has exclusively discussed the current state of art in MD based simulations of BN nanofillers either in pristine or defective form. But some progress has also been made in simulating the hybrids of BN nanofillers with polymers. Liew and Yuan [202] investigated the structural performance of double-walled nanotube consisting of a carbon nanotube inside a boron nitride nanotube. Liew and Yuan performed these simulations in MD framework in combination with universal force field [164, 203]. During their simulations, the nanotubes were subjected to axial compressive loading. It was reported in their simulations that at the annealing temperatures of 3500°K and 4000°K, distortion and critical buckling load of the inner CNTs were dependent on the chiral vector.

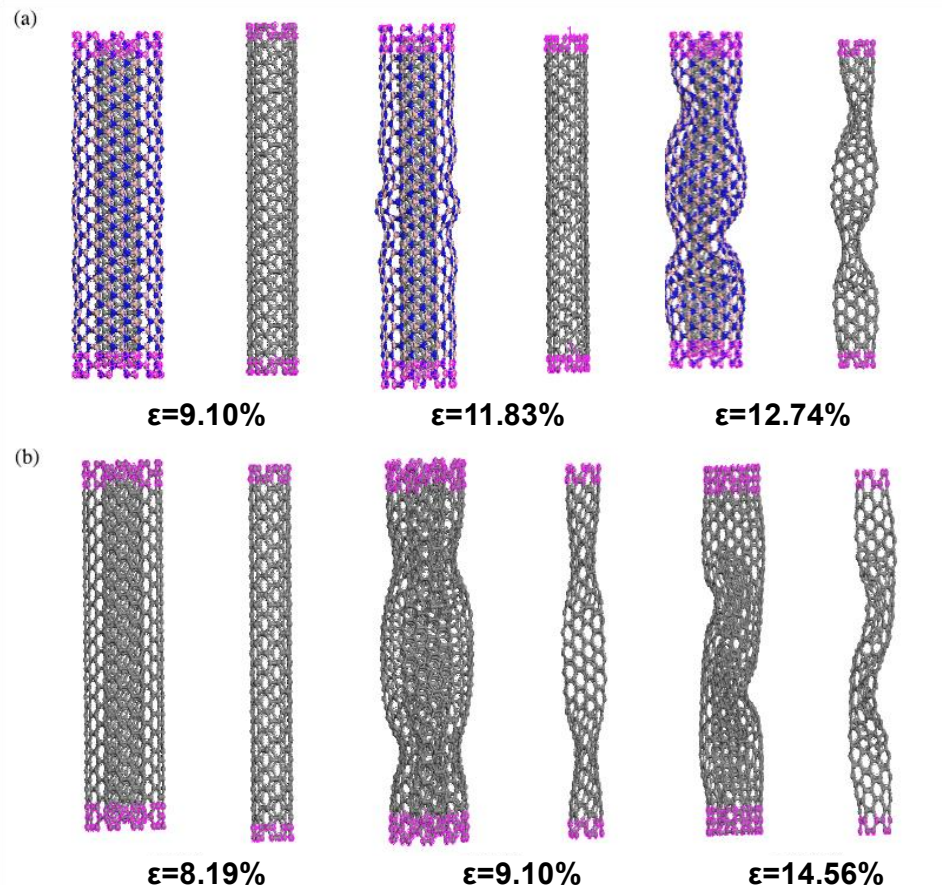

Fig. 16. Coaxial nanotubes: (a) Optimized C(5, 5)@BN(10, 10) (b) Optimized C(5, 5)@C(10, 10) at different axial compressive strains (ε) at the temperature of 300^0 K. (Reproduced with permission from [202])

It can be inferred from **Fig. 16** that in case of C(5, 5)@BN(10, 10) outer BNNT starts showing instability at ε=11.83% while the inner carbon nanotube remains stable till the higher values of strains (12.74%). But in case of C(5, 5)@C(10, 10), both tubes became unstable simultaneously at lower strain values (9.10%) than the previous case. Hence it can be concluded from the work Liew and Yuan [202] that BNNT acts as a better protection than a CNT when used as an outer protection tube.

Table 4. FWHM values of single, bilayer and trilayer sheets of graphene and BNNS.

Material	*FWHM (1st Peak)*	*FWHM (2nd Peak)*	*FWHM (3rd Peak)*
Gr (monolayer)	0.00258 nm	0.00221 nm	0.00257 nm
Gr-Gr (bilayer)	0.00236 nm	0.00225 nm	0.00234 nm
Gr-Gr-Gr (trilayer)	0.00231 nm	0.00201 nm	0.00255
BN(monolayer)	0.00301 nm	0.00217 nm	0.0301 nm
BN-BN (bilayer)	0.00302 nm	0.00219 nm	0.00311 nm
BN-Gr-BN (sandwich)	0.00221 nm	0.00184 nm	0.00255 nm

Yuan et al. [204-205] investigated the structural stability and elastic properties of bilayer and trilayer graphene and boron nitride nanosheets by employing MD based simulations in conjunction with universal force field [164]. Their investigation on multiplayers of nanosheets was based on analyzing and comparing the binding energy, van der Waals interactions between layers and radial distribution function (RDF). In their computational model the full width half maximum (FWHM) of RDF was considered closely related to the integrity of the atomistic structure. The structures with sharp peaks and smaller values of FWHM for RDF were predicted to possess better integrity. They performed simulations with bilayers and trilayers of nanosheets, and compared the results with the monolayer of graphene and BNNS. FWHM values obtained from first, second and third peaks (refer to **Table 4**) suggested a less deviation between bilayer and single sheet of BNNS, and also these changes in values of FWHM for BNNS are comparatively lower as compared to graphene. These trends in FWHM between single and

bilayers indicates that bilayer BNNS can be considered as more integrated structure as compared to graphene [204].

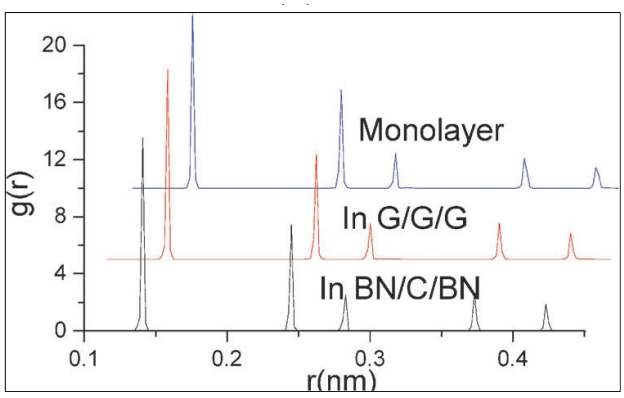

Fig. 17. RDF for monolayer graphene, three layers of graphene and sandwich structure of graphene sheet between BNNS (Reproduced with permission from [205]).

Young's moduli of the combined bilayer nanosheets were found to be lower than that of corresponding monolayers for graphene and BNNS. In case of BN nanosheets, the reduction in the Young's modulus was less as compared to that of graphene nanosheets. Yuan and Liew [205] also performed MD simulations to investigate the structure stability and high temperature distortion-resistance of a sandwich structure of graphene and BN nanosheets. The optimal interlayer equilibrium distances between graphene nanosheets (in case of graphene sandwich) and graphene and BN nanosheets (in case of BNNS-graphene sandwich) were reported as 0.347 nm and 0.341nm, respectively. Equilibrium distance was the spacing between nanosheets at which repulsive and attractive forces are zero. It was further predicted in their work that graphene sandwiched between BN nanosheets proved to be a more integrated structure as compared to monolayer graphene sandwiched between graphene nanosheets in a crystal structure on the bases of FWHM values obtained from the first peak in RDF as provided in **Table 4** and illustrated in **Fig. 17**.

Song and Medhekar [206] also studied the hybrid nanostructures of graphene and h-BN nanoribbons. In their MD based simulations, interatomic interactions were modeled with the help of Tersoff potential [136] with optimized parameters taken from the work of Matsunaga et al. [149]. The thermal transport in the direction perpendicular to the interface was reported to be less affected by the composition. On the other hand, it was also concluded in their work that thermal transport in these hybrid nanoribbons was significantly affected by the interface scattering and the presence of the low thermal conductivity component i.e. h-BN in the path of the thermal current. Whereas thermal transport parallel to the interface was limited by the graphene component. Shen Haijun [207] investigated the compressive strength of single-walled BNNT and hybrid structure of BNNT embedded into CNT. The simulations were performed using B-N potential parameters from Albe et al. [150] while non-bonded interactions were treated with the help of LJ potential parameters [164]. It can be inferred from their conclusions that hybrid structures show higher compressive strength as well as melting temperature as compared to single BNNT. In 2013, Zhao and Xue [160] examined the mechanical properties of hybrid structure of graphene and h-BN. While B-N, B-C and N-C interactions were modeled by mixing of potential parameters of Matsunaga et al. [148], parameters provided by Lindsay and Broido [196] were used to model carbon-carbon interactions. Hybrid sheets were predicted to show plastic behavior that was absent in pure h-BN and graphene nanosheets. Young's modulus for hybrid nanosheets showed a decreasing trend with increasing concentration of BN, irrespective of BN shapes and distribution. DFT based simulations have also been employed to investigate the hybrid structures of BN nanofillers. Zhang et al. [208] investigated the electronic and transport properties of fullerene and vanadium based peapod of BNNTs using DFT calculations. Based on their simulation results, BNNT based peapod was predicted to be semiconducting with

a narrow bandgap. Further details regarding this behavior of BNNTs can be found in their paper [208].

Nanocomposites:

So far, this review paper has exclusively discussed nanostructures such as BN nanotubes, BN nanosheets and hybrid structures of these BN nanofillers with graphene or CNT. But decent amount of progress has also been made in simulating BN nanofiller based nanocomposites. This section is focused on the MD based simulations of BN nanocomposites. Nasrabadi and Foroutan [209] used MD based simulations for investigating the interfacial binding of BN nanotubes with poly[m-phenylenevinylene-co-(2,5-dioctyloxy-p-phenylenevinylene)] PmPV, polystyrene, and polythiophene. In their simulations, MM3 [210] and Lennard Jones force field have been employed for simulating the bonded and non-bonded interactions (interface), respectively. From their simulations, it can be inferred that interaction energy of BNNT- polymer composites is strongly influenced by specific monomer structure and nanotube radius. On the basis of higher values of interaction energy of BNNT-polymer composites, they suggested that the BNNTs could be more efficient nano-filler than the CNTs for nano-composite reinforcement applications. Effect of polarization of BNNT on the interfacial strength was also studied in the same work [209] and it was concluded that interfacial strength was increased due to polarization of BNNTs.

Fatemi and Foroutan [211] investigated the dispersion of two BNNTs in aqueous solution of triton X-100 as surfactant, using MD based simulations in combination with AMBER99 force field [212]. The presence of the surfactant resulted into an increase in surface angle between the two nanotubes and hence more gap created between two BNNTs leading to the dispersion of the

BNNTs. The presence of the surfactant, shortened the bond distance between nitrogen atom of the BNNT and hydrogen atom of water molecules. Moreover, the estimated values of radius of gyration of the surfactant and the interfacial angle between two BNNTs shed more light on the arrangement of the surfactants around the BNNTs with and without the presence water molecules.

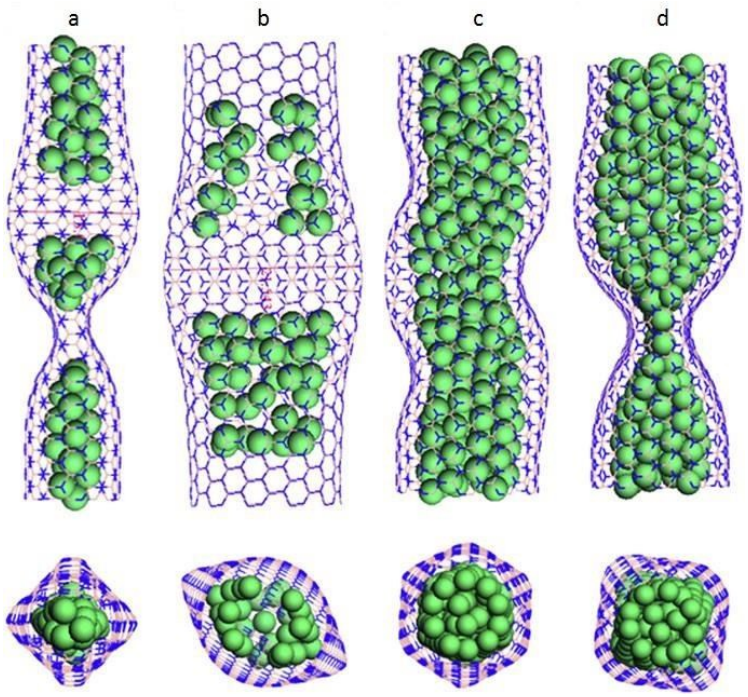

Fig. 18. Deformation pattern of (a) 49 Cu @ BNNT(7,7) (b) 49Cu@ BNNT(11,11) (c) 195CuBNNT(11,11) at a simulation time t (d) 195Cy@ BNNT(11,11) after an increased simulation time t+Δt. (Reproduced with permission from Wang et al. [213]).

Wang and his team [213] applied axial compression on copper-filled BNNT to study buckling behavior of BNNTs using the MD framework. Universal force field, with parameters taken from the work of Jung et al. [214] and Zhou et al. [215] were used for simulating the atomic interactions between the atoms. It was observed that nanotubes with different chirality exhibited different deformation patterns and energy loss. Side and top views for different tubes at buckling

stage, have been shown in **Fig. 18**. **Fig. 18(a)** shows a 49 Cu@ BNNT (7, 7) i.e. 49 copper atoms in BNNT (7, 7), **Fig. 18(b)** is for 49 Cu@ BNNT (11, 11), both showing different deformation patterns. **Fig. 18(c)** and **Fig. 18(d)** depicted the same atomic configuration i.e. 195 Cu@ BNNT (11, 11) nanotube, but at different simulation steps. It is clear from these two figures that a regular hexahedron like shape evolved before buckling of the tube and at the time of buckling, this shape finally transformed to a square shape. In addition to these deformation patterns, BN nanotubes filled with larger number of copper atoms were found to be more stable as compared to the nanotubes filled with smaller number of copper atoms.

Bari et al. [216] carried out MD simulations to study the non-covalent interactions between polyvinyl pyrrolidone (PVP) and isolated BNNSs in water medium. Interactions between the PVP molecule and water atoms were treated with general AMBER force field [217-218] while the LJ potential was used to take care of the interactions between the BNNSs and water with parameters from the work of Mayo et al. [219]. It was predicted in their research that in the initial stages of simulation, PVP chains showed a random thermal motion in water, and finally reached within an approachable distance to BNNS, so that, interactions could be possible between BNNS and PVP. It can be inferred from their conclusion that after the chain reach within close proximity to BNNS, the distance between these two doesn't change any further. This emphasized that in the presence of water, there exists a strong affinity between the PVP chain and the BNNS. Griebel and Hamaekers [220] examined the elastic properties of BNNT embedded into amorphous silicon-boron-nitride ceramics. The computational work was performed using Parrinello–Rahman approach [178, 221] with potential parameters from the work of Matsunaga et al. [147]. The results obtained in their computational model further suggested that out of Si3BN5, Si3B2N6 and Si3B3N7 matrices, Si3B3N7 had the highest Young

modulus with the highest elastic range. Further examination of the properties of a ceramic composite material made of Si3B3N7 as matrix and BN nanotubes as filler was performed in the computational work of Griebel and Hamaekers [220]. It was further suggested that the simple macroscopic rule-of-mixture, which just accounts for the volume fraction of the nanotube could be used for composites with periodically infinite long BN nanotubes.

Thomas and his team [222] studied the interactions of BNNT and CNTs embedded into lipid bilayers. They employed MD based simulations in conjunction with CHARMM36 force field parameters [223-224] for investigating the interaction of BNNT and CNT with lipid bilayers. It was predicted in their simulations that the stability of BNNTs in cell membranes was comparable to that of functionalized CNTs. It was further observed in their simulations that a narrow BNNT might be blocked at one end by lipid molecules as indicated in **Fig. 19(a)**, while a wider BNNT was only partially blocked by lipid molecules as shown in **Fig. 19(b)**. On the other hand, CNT was reported to be completely occupied by lipid molecules as illustrated in **Fig. 19(c)**. Yuan and Liew [225] examined the strength of coaxially placed silicon wire (SiNW) inside a BN nanotube. MD based studies were performed in conjunction with universal force field [147,199] to investigate the effect of silicon nanowire on the structural strength of BN nanotubes. Two different type of silicon nanowires (SiNWs) were simulated by Yuan and Liew in their atomistic model as shown in **Fig. 14**. Axial monatomic chain with a helical shell of SiNWs, coaxially aligned inside a BNNT (10, 10) and only an axially aligned monatomic chain of SiNW inside the BNNT (5, 5) are shown in **Fig. 14(a) & (b)** and **Fig.14(c) & (d)**, respectively. It was reported in their work that BNNT and SiNW nanocomposites were more stable as compared to their respective pristine forms. It was also concluded in their research work that the deformation

pattern and energy loss varied from form to form, whereas the buckling strain remained same for the pristine BNNT and BNNT/ Si NW composite.

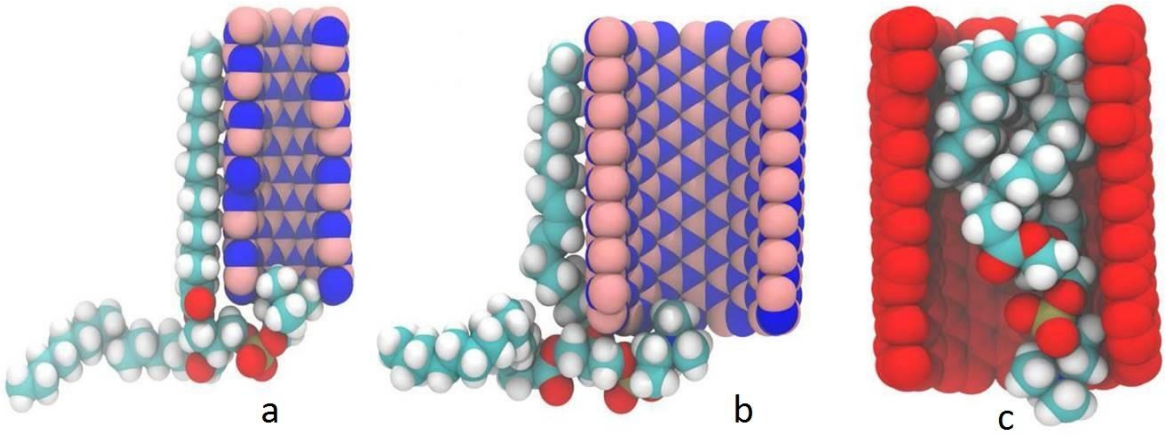

Fig. 19. **(a)** Blocked lipid at the end of narrow BNNT **(b)** partially blocked lipid along with a wider BNNT **(c)** completely occupied CNT with the lipid molecules. (Reproduced with permission from Thomas et al. [222]).

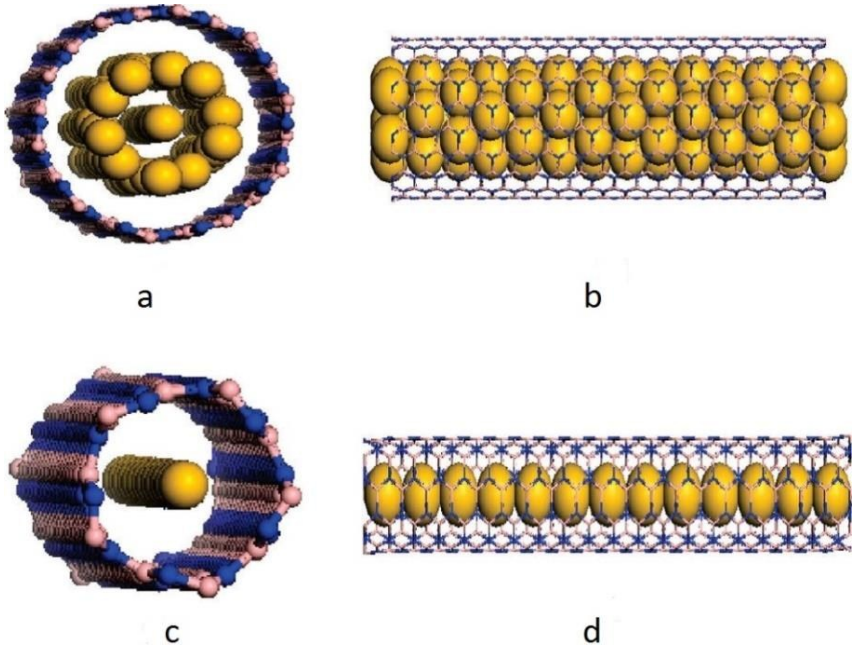

Fig. 20. **(a)** Axial monatomic and helical shell of silicon nanowires coaxially aligned inside the BNNT (10,10) **(b)** side view of atomic configuration shown in part **(a)**. **(c)** Only a monatomic chain of silicon nanowire inside BNNT (5, 5) **(d)** side view of atomic configuration shown in part **(c)**. (Reproduced with permission from Yuan and Liew [225]).

Table 5. Compilation of different type of potentials employed in different molecular dynamics based simulations to predict the mechanical and thermal behavior of BN nanofillers.

Potential Parameters	Any Modification	Ref.	Work Done
Albe et al. [150]	-	[157]	Effect of temperature and strain rate on mechanical properties of BNNS
	-	[169]	Radial compression of BNNTs
	-	[171]	Bending rigidity of BNNSs
	-	[183]	Structural and thermal behavior of BNNTs with SW defects
	-	[184]	Fracture and buckling behavior of BNNTs
	-	[188]	Torsional vibrational performance of BNNTs
	-	[189]	Torsional and buckling behavior of BNNTs
	-	[191]	Effect of interfacial structure on mechanical properties of BNNBs
	-	[194]	Effect of diameter and temperature on thermal conductivity of BNNTs, Tensile properties of BNNTs
	-	[201]	Effect of temperature and diameter on coefficients of thermal (CTE) expansion of BNNTs
	-	[207]	Thermal-stability and compressive behavior BNNT and BNNT@CNT
Sevik et al. [146]	-	[146]	Characterization of thermal transport in BN nanofillers
	Cut-off function f(r)=1	[161]	Effects of vacancy and SW defects on mechanical properties of BNNSs
	Tersoff-Brenner potential	[181]	Effect of vacancy and SW defects on failure behavior of BNNTs under tension
	-	[187]	Effect of chirality on elastic properties of BNNTs under tension and torsion
	$\mathbf{R_{ij}=S_{ij}}$	[190]	Size effects on mechanical properties of BNNRs
	-	[197]	Thermal conductivity of graphene-BNNS hybrids
	-	[199]	Impact of isotopes on thermal transport in BN nanostructures
Matsunaga et al. [147]	-	[159]	Investigation of tensile properties and thermal conductivity of BNNS
	-	[160]	Mechanical properties of hybrid graphene and BNNS
	Inclusion of attractive potential term to deal with homo-elemental bonds	[177]	Effects of vacancies and functionalization on Young's modulus of BNNTs
	-	[182]	Mechanical properties of polycrystalline BNNSs
	-	[206]	Thermal transport in hybrid of graphene and h-BN
	-	[220]	Elastic properties of BNNTs embedded in amorphous Si-B-N

Sekkal et al. [145]	Slightly modified to get better fit to the bond length and bond energy	[26]	Elastic and shear moduli of BN nanofillers
Liao et al. [168]	Modified version of parameters from Albe et al. to, better capture of properties of nanofillers, predict better bond breaking behavior	[168]	Deformation behaviors of BNNTs under axial tensile Strains in armchair direction
	-	[167]	Buckling behavior of pristine and hydrogenated BNNTs
	-	[172]	Effect of temperature on tensile and compressive behavior of BNNTs
UFF & Dreiding	-	[163]	Mechanical properties of hydrogenated BNNTs
	-	[174]	High-Temperature Thermal Stability and In-Plane Compressive Properties of a BNNT
	-	[202]	High-temperature thermal stability and axial compressive properties of a coaxial CNT @BNNT
	-	[205]	Structure stability and high-temperature distortion resistance of trilayer hybrid of graphene and BNNS
	-	[204]	Structural Stability and Elastic Properties of Bilayer hybrid of Graphene and BNNS
	-	[213]	Axial compression of copper-filled BNNT
	-	[225]	Compressing behavior of coaxial Silicon Nanowires inside a BNNT
Harmonic potential or LJ potential	Harmonic potential for bonded interactions and LJ potential non-bonded interactions	[170]	Buckling behavior of BNNTs under axial compression
	Parameters from Liao et al. were used to obtain harmonic potential parameters for bonded interactions	[179]	Effects of vacancy defects on the compressive buckling of boron nitride nanotubes
ReaxFF	-	[180]	Point and line defects on BNNTs
	-	[186]	Fracture behavior of defective BNNTs
MM3+LJ	-	[209]	Interactions between Polymers SWBNNT
AMBER Force Field + LJ	-	[211]	Dispersion of BNNTs inside water by triton X-100 surfactant
	-	[216]	Liquid phase exfoliation and crumpling of BNNSs
CHARM M36 force field	-	[222]	Stability of BNNTs into Lipid bilayers

It can be inferred from the preceding review that Tersoff is the most common among the potentials for simulating interatomic interactions in BN nanofillers. In addition to Tersoff type potential, ReaxFF, Harmonic, LJ, MM3, AMBER and CHARM potentials were also employed by few researchers for the modeling of BN nanofillers. A summary of different type of potentials employed in various MD simulations for estimating the mechanical and thermal behavior of BN nanofillers is provided in **Table 5**.

Conclusion and future aspects

In this review, authors have summarised recent progress made in the field of atomistic modeling of BN nanofillers. Due to exceptional properties, BN nanofillers are emerging as a potential candidate for wide range of practical applications. On the basis of wide band gap in the range of ~5.5eV, higher stability against oxidation even at higher temperatures and thermal stability of BN nanofillers have made them superior to carbon based nanofillers for specific applications and hence their further exploration has always drawn attention of researchers.

From the preceding review on atomistic modeling of BN nanofillers, it can be concluded that these approaches are capable of producing results that are in good agreement with experimental results. When compared with each other, each of these techniques has its own advantages along with certain limitations associated with it, as discussed in the review. In spite of the fact that DFT based simulations are more accurate, but has limitations of being computationally intensive and limits overall system size. Although, tight binding calculations are faster but needs further improvements like scalability. Continuum based FEM techniques proved accurate for predicting the global properties, but have limitations while modeling the localised effects such as bond formation and rotation in atomistic atmosphere. When it comes to MD, Tersoff type potentials have generated more attention among the researchers for simulating the bonded interactions, due

to accurate parameterizations that produces accurate fit with the DFT calculations and experimental results. So far, different set of Tersoff type potential parameters have been proposed by the researchers. Sekkal et al. [145], Sevik et al. [146], Matsunaga et al. [147] and Albe et al. [150] are the prominent contributors for these parameters. Due to empirical nature of these parameters, an overall scattered results in terms of mechanical, fracture and thermal properties has been reported in MD based simulations performed with these parameters. Some studies [21, 161] on mechanical properties of BN nanofillers with minor modifications in cut-off function have predicted better results that are in good agreement with DFT and experiments. These studied were performed using the parameters from Sevik et al. [146]. However, no study with other set of parameters, used in conjunction with modified cut-off function, has been reported yet. So, a scope of further improvements, such as cut-off function optimisation, exists, as far as MD simulations of BN nanofillers are concerned.

Overall, atomistic modeling and simulation techniques are proving to be an excellent complement to the experimental techniques to explore further research directions. Properties which cannot be explored with experiments, can be traceable using these techniques and hence, further improvements in these techniques will make them more versatile.

References:

1. Rubio A, Corkill JL, Cohen ML. Theory of graphitic boron nitride nanotubes. Phys. Rev. B 1994; 49: 5081–84.

2. Chopra NG, Luyken RJ, Cherrey K, Vincent HC, Marvin LC, Steven GL, Zettl A. Boron nitride nanotubes. Science 1995; 269: 966–67.

3. Corso M, Auwärter W, Muntwiler M, Tamai A, Greber T, Osterwalder J. Boron Nitride Nanomesh. Science 2004; 303: 217-20.

4. T. Sato- Studies on hexagonal and rhomobohedral layered boron nitrides: synthesis, crystal growth, and transformation under high pressure, *Report of National Institute for Research in Inorganic Materials*, Tsukuba, Japan, **1987**.

5. Pouch JJ, Alterovitz SA. Synthesis and properties of boron nitride. Mater. Manuf. Processes 1990; 6: 373-74.

6. Iijima S. Helical microtubules of graphitic carbon. Nature 1991; 354: 56-58.

7. Novoselov KS, Geim AK, Morozov SV, Jiang D, Zhang Y, Dubonos SV. Electric Field Effect in Atomically Thin Carbon Films. Science 2004; 306: 666–69.

8. Novoselov KS, Jiang D, Schedin F, Booth TJ, Khotkevich VV, Morozov SV. Two-dimensional atomic crystals. Proc. Natl. Acad. Sci. U. S. A. 2005; 102: 10451-53.

9. Blas´e X, Rubio A, Louie SG, Cohen ML. Stability and band gap constancy of boron nitride nanotubes. Europhys.Lett. 1994; 28: 335-40.

10. Watanabe K, Taniguchi T, Kanda H- Direct. Bandgap Properties And Evidence For Ultraviolet Lasing of Hexagonal Boron Nitride Single Crystal. Nat. Mater. 2004; 3: 404 - 09.

11. Lin Z, Liu Y, Moon K, Wong C. Enhanced thermal transport of hexagonal boron nitride filled polymer composite by magnetic field-assisted alignment. Electronic Comp. and Tech. Conf. (ECTC), 2013 IEEE 63rd, 1692-96.

12. Yung K C, H. Liem H. Enhanced thermal conductivity of boron nitride epoxy-matrix composite through multi-modal particle size mixing. J. Appl. Polym. Sci. 2007 Vol. 106: 3587–91.

13. Huang X, Wang S, Zhu M, Yang K, Jiang P, Bando Y, Golberg D, Zhi C. Thermally conductive, electrically insulating and melt-processable polystyrene/boron nitride nanocomposites prepared by in situ reversible addition fragmentation chain transfer polymerization. Nanotechnology 2015; 26: 015705.

14. Wong CP, Raja S. Bollampally. Comparative study of thermally conductive fillers for use in liquid encapsulants for electronic packaging. IEEE Trans. Adv. Packag. 1999; 22: 54-59.

15. Golberg D, Pedro MF, J. Costa J, Lourie O, Masanori Mitome M , Xuedong Bai X, Kurashima K, Zhi C, Tang C, Bando T. Direct Force Measurements and Kinking under Elastic Deformation of Individual Multiwalled Boron Nitride Nanotubes. Nano Lett. 2007; 7: 2146-51.

16. Arenal R, Wang M, Xu Z, Loiseau A, Golberg D - Young Modulus. Mechanical and Electrical Properties of Isolated Individual and Bundled Single-Walled Boron Nitride Nanotubes. Nanotechnology 2001; **22:** 26570.

17. Kudin KN, Scuseria GE, Yakobson BI. C2F, BN, and C Nanoshell Elasticity from Ab Initio Computations. Phys Rev B 2001; 64:235406.

18. Sahin H, Cahangirov S, Topsakal M, Bekaroglu E, Akturk E, Senger RT, Ciraci S. Monolayer Honeycomb Structures Of Group-IV Elements And III–V Binary Compounds:First-Principles Calculations. Phys Rev B 2009; 80:155453.

19. Andrew RC, Mapasha RE, Ukpong AM, Chetty N- Mechanical Properties of Graphene and Boronitrene. Phys Rev B 2012; 85:125428.

20. Peng Q, Ji W, De S. Mechanical properties of the hexagonal boron nitride monolayer: ab initio study. Comput Mater Sci 2012; 56:11-17.

21. Le MQ. Atomistic study on the tensile properties of hexagonal AlN, BN, GaN, InN and SiC sheets. J. Comput. Theor. Nanosci. 2014; 11: 1458-64.

22. Le MQ. Young's Modulus Prediction of Hexagonal Nanosheets and Nanotubes Based on Dimensional Analysis and Atomistic Simulations. Meccanica, 2014; 49: 1709-19.

23. Chopra NG, Zettla A. Measurement of the elastic modulus of a multi-wall boron nitride nanotube, Solid State Commun. 1998; 105: 297-300.

24. Suryavanshi AP, Yu MF, Wen J, Tang C, Bando Y. Elastic modulus and resonance behavior of boron nitride nanotubes, Appl. Phys. Lett. 2004; 84: 2527.

25. Fakhrabada DV, Shahtahmassebia N. First-principles calculations of the Young's modulus of double wall boron-nitride nanotubes. Mat. Chem. and Phys. 2013; 138: 963–66.

26. Verma V, Jindal VK, Dharamvir K. Elastic Moduli of A Boron Nitride Nanotube. Nanotechnology 2007; 18: 435711.

27. Ouyang T, Chen Y, Xie Y, Yang K, Bao Z, Zhong J. Thermal transport in hexagonal boron nitride nanoribbons. Nanotechnology 2010; 21: 245701.

28. Chen Y, Zou J, Campbell SJ, Caer GL. Boron Nitride Nanotubes: Pronounced Resistance to Oxidation. Appl. Phys. Lett. 2004; 84: 2430.

29. Bundy FP, Wentorf RH. Direct Transformation of Hexagonal Boron Nitride to Denser Forms. J. Chem. Phys. 1963; 38: 1144.

30. Kubota Y, Watanabe K, Tsuda O, Taniguchi T. Deep ultraviolet light-emitting hexagonal boron nitride synthesized at atmospheric pressure. Science 2007; 317: 932-34.

31. Noor-A-Alam M, Kima HJ, Shin YH. Dipolar polarization and piezoelectricity of a hexagonal boron nitride sheet decorated with hydrogen and fluorine. Phys. Chem. Chem. Phys. 2014; 16: 6575-82.

32. Michel KH, Verberck B. Theory of elastic and piezoelectric effects in two-dimensional hexagonal boron nitride. Phys. Rev. B 2009; 80: 224301.

33. Qi J, Qian X, Qi L, Feng J, Shi D, Li J. Strain-Engineering of Band Gaps in Piezoelectric Boron Nitride Nanoribbons. Nano Lett. 2012 12: 1224–28.

34. Huang Q, Bando Y, Zhao L, Zhi CY, Golberg D. pH Sensor Based On Boron Nitride Nanotubes. Nanotechnology 2009; 20: 415501.

35. Panchal MB, Upadhyay SH- Boron. Nitride Nanotube-Based Bio-sensing of Various Bacterium/Viruses: Continuum Modeling-Based Simulation Approach. "IET Nanobiotechnol. 2014; 8:143-48.

36. Chowdhury R, Adhikari S. Boron-Nitride Nanotubes as Zeptogram-Scale Bio-nano-sensors: Theoretical Investigations. Nanotechnology, IEEE Transactions 2010; 10: 659-67.

37. Panchal MB, Upadhyay SH. Boron nitride nanotube-based biosensor for acetone detection: molecular structural mechanics-based simulation. Mol. Simul. 2014; 40: 103542.

38. Panchal MB, Upadhyay SH, Harsha SP. Mass Detection Using Single Walled Boron Nitride Nanotube as A Nanomechanical Resonator. Nano 2012; 07: 1250029.

39. Panchal MB, Upadhyay SH. Single walled boron nitride nanotube-based biosensor: an atomistic finite element modeling approach. IET Nanobiotechnol. 2014; 8:149-56.

40. Chen X, Wu P, Rousseas M, Okawa D, Gartner Z, Zettl A, Bertozzi CR. Boron Nitride Nanotubes Are Noncytotoxic and Can Be Functionalized for Interaction with Proteins and Cells. J. Am. Chem. Soc. 2009; 13: 890-91.

41. Ciofania G, Raffaa V, Menciassia A, Cuschieria A. Boron nitride nanotubes: An innovative tool for nanomedicine. Nanotoday 2009; 4: 8–10.

42. Ciofani G, Danti S, Genchi GG, Mazzolai B, Mattoli V. Boron nitride nanotubes: biocompatibility and potential spill-over in nanomedicine. Small, 2013; 9: 1672–85.

43. Shelimov KB, Moskovits M. Composite Nanostructures Based on Template-Grown Boron Nitride Nanotubules. Chem. Mater. 2000; 12: 250-54.

44. Zhi C , Bando Y, Tang C, Honda S, Sato K, Kuwahara H, Golberg D. Characteristics of Boron Nitride Nanotube–Polyaniline Composites. Angew. Chem. Int. Ed. 2005; 44: 7929-32.

45. Zhou W, Qi S, An Q, Zhao H, Liu N. Thermal conductivity of boron nitride reinforced polyethylene composites. Mater. Res. Bull. 2007; 42:1863-73"

46. Ishida H, Rimdusit S. Very high thermal conductivity obtained by boron nitride-filled polybenzoxazine. Thermochimica Acta, 1998; 320: 177-86"

47. Zhoua W, Qia S, Lib H, Shaoa S. Study on insulating thermal conductive BN/HDPE composites. Thermochim. Acta 2007; 452: 36–42".

48. Yi M, Shen Z, Lei Liua L, Lianga S. Size-selected boron nitride Nanosheets as oxygen-atom corrosion resistant fillers. RSC Adv. 2015; 5: 2983-87".

49. Xuebin Wang, Amir Pakdel, Jun Zhang, Qunhong Weng, Tianyou Zhai, Chunyi Zhi, Dmitri Golberg, Yoshio Bando, "Large-surface-area BN nanosheets and their utilization in polymeric composites with improved thermal and dielectric properties. Nanoscale Res. Lett. 2012, 7:662.

50. Ciofani G, Danti S, Ricotti L, D'Alessandro D, Moscato S, Berrettini S, Mattoli V, Menciassi A. Boron Nitride Nanotubes: Production, Properties, Biological Interactions and Potential Applications as Therapeutic Agents in Brain Disease. Current Nanoscience 2011; 7: 94-109.

51. Ciofani G. Potential Applications of Boron Nitride Nanotubes As Drug Delivery Systems. Expert Opin. Drug Delivery 2010; 7:889-93.

52. Li X, Zhi C, Hanagata N, Yamaguchi M, Bandoa Y, Golberg D. Boron Nitride Nanotubes Functionalized With Mesoporous Silica For Intracellular Delivery Of Chemotherapy Drugs. Chem. Commun. 2013; 49: 7337-39.

53. Ferreira T. H., Soares D. C. F., Moreira L. M. C., da Silva P. R. O., dos Santos R. G., de Sousa E. M. B. Boron nitride nanotubes coated with organic hydrophilic agents: stability and cytocompatibility studies. Mater. Sci. Eng.: C 2013; 33: 4616-23.

54. Del Turco, S., Ciofani, G., Cappello, V., Gemmi, M., Cervelli, T., Saponaro, C., Mattioli, V. Cytocompatibility evaluation of glycol-chitosan coated boron nitride nanotubes in human endothelial cells. Colloids and Surf. B, 2013; 111: 142-149.

55. Ferreira T. H., Hollanda, L. M., Lancellotti, M., de Sousa, E. M. B. Boron Nitride Nanotubes Chemically Functionalized with Glycol Chitosan for Gene Transfection in Eukaryotic Cell Lines. J. Biomed. Mater. Res. Part A 2015; 103: 2176-85.

56. Ciofani, G., Raffa, V., Menciassi, A., Cuschieri, A Folate Functionalized Boron Nitride Nanotubes and their Selective Uptake by Glioblastoma Multiforme Cells: Implications for their Use as Boron Carriers in Clinical Boron Neutron Capture Therapy. Nanoscale Res. Lett. 2009; 4:113-21.

57. Jhi, S. H., Kwon, Y. K. Hydrogen adsorption on boron nitride nanotubes: A path to room-temperature hydrogen storage. Phys. Rev. B 2004; 69: 245407.

58. Zhang, H., Tong, C. J., Zhang, Y., Zhang, Y. N., Liu, L. M. Porous BN for hydrogen generation and storage. *J. Mater. Chem. A*, 2015; 3: 9632-37.

59. Lei, W., Zhang, H., Wu, Y., Zhang, B., Liu, D., Qin, S., Chen, Y. Oxygen-doped boron nitride nanosheets with excellent performance in hydrogen storage. Nano Energy 2014; 6: 219-24.

60. Lee C, Li Q, Kalb W, Liu XZ, Berger H, Carpick RW, Hone J. Frictional characteristics of atomically thin sheets. Science 2010; 328: 76-80.

61. Lin, Y., Bunker, C. E., Fernando, K. S., Connell, J. W. Aqueously Dispersed Silver Nanoparticle-Decorated Boron Nitride Nanosheets for Reusable, Thermal Oxidation-Resistant Surface Enhanced Raman Spectroscopy (SERS) Devices. ACS Appl. Mater. Interfaces 2012; 4:1110–17.

62. Watanabe, K., Taniguchi, T., Niiyama, T., Miya, K., Taniguchi, M. Far-ultraviolet plane-emission handheld device based on hexagonal boron nitride. Nat. Photonics 2009; 3: 591-94.

63. Haubner, R., Wilhelm, M., Weissenbacher, R., Lux, B. Boron Nitrides- Properties, Synthesis and Applications, in High Performance Non-Oxide Ceramics II. Struct. Bond. 2002; 102: 1-45.

64. Lei, W., Portehault, D., Dimova, R., Antonietti, M. Boron Carbon Nitride Nanostructures from Salt Melts: Tunable-Soluble Phosphors. J. Am. Chem. Soc. 2011; 133: 7121-27.

65. Li, L. H., Chen, Y., Cheng, B. M., Lin, M. Y., Chou, S. L., Peng, Y. C. Photoluminescence of boron nitride nanosheets exfoliated by ball milling. Appl. Phys. Lett. 2012 100: 261108.

66. Guo, G. Y., Lin, J. C. Systematic ab initio study of the optical properties of BN nanotubes. Phys. Rev. B 2005; 71: 165402.

67. Miyoshi, K., Buckley, D. H., Pouch, J. J., Alterovitz, S. A., Sliney, H. E . Mechanical strength and tribological behavior of ion-beam-deposited boron nitride films on non-metallic substrates. Surf. Coat. Technol. 1987; 33: 221–33.

68. Pawlak, Z., Kaldonski, T., Pai, R., Bayraktar, E., Oloyede, A. A comparative study on the tribological behaviour of hexagonal boron nitride (h-BN) as lubricating micro-particles-An additive in porous sliding bearings for a car clutch. Wear 2009 267: 1198-1202.

69. Lahiri, D., Singh, V., Benaduce, A. P., Seal, S., Kos, L., Agarwal, A. Boron nitride nanotube reinforced hydroxyapatite composite: Mechanical and tribological performance and *in-vitro* biocompatibility to osteoblasts. J. Mech. Behav. Biomed. Mater. 2011; 4: 44–56.

70. Lei, W., Portehault, D., Liu, D., Qin, S., Chen, Y. Porous boron nitride nanosheets for effective water cleaning. Nature Commu. 2013; 4:1777.

71. Smith, M. W., Jordan, K. C., Park, C., Kim, J. W., Lillehei, P. T., Crooks, R., Harrison, J. S. Very long single- and few-walled boron nitride nanotubes via the pressurized vapor/condenser method. Nanotechnology 2009; 20:505604.

72. Pacile, D., Meyer, J. C., Girit, C. O., Zettl, A. The two-dimensional phase of boron nitride: Few-atomic-layer sheets and suspended membranes. Appl. Phys. Lett. 2008; 92: 133107.

73. Novoselov, K. S., Jiang, D., Schedin, F., Booth, T. J., Khotkevich, V. V., Morozov, S. V., Geim, A. K. Two-dimensional atomic crystals. PNAS 2005; 102: 10451-53.

74. Han, W. Q., Wu, L., Zhu, Y., Watanabe, K., Taniguchi, T. Structure of chemically derived mono- and few-atomic-layer boron nitride sheets. Appl. Phys. Lett. 2008; 93: 223103.

75. Song L, Ci L, Lu H, Sorokin PB, Jin C, Ni J, Kvashnin AG, Kvashnin DG, Lou J, Yakobson BI, Ajayan PM. Large scale growth and characterization of atomic hexagonal boron nitride layers. Nano Lett. 2010; 10: 3209-15.

76. Ci L, Song L, Jin C, Jariwala D, Wu D, Li Y, A rivastava S, Wang ZF, Storr K, Balicas L, Liu F, Ajayan. Atomic layers of hybridized boron nitride and graphene. Nat.Mater. 2010; 9: 430-35.

77. Shi Y, Hamsen C, Jia X, Kim KK, Reina A, Hofmann M, Hsu AL, Zhang K, Li H, Juang ZY, Dresselhaus MS, Li LJ, Kong J. Synthesis of few-layer hexagonal boron nitride thin film by chemical vapor deposition. Nano Lett. 2010; 10: 4134-39.

78. Gao R, Yin LW, Wang CX, Qi YX, Lun N, Zhang L, Liu YX, Kang L , Wang. High Yield Synthesis of Boron Nitride Nanosheets with Strong Ultraviolet Cathodoluminescence Emission. J. Phys. Chem. C. 2009 113; 15160-65.

79. Kim, K. K., Hsu, A., Jia, X., Kim, S. M., Shi, Y., Hofmann, M., ... Kong, J . Synthesis of Monolayer Hexagonal Boron Nitride on Cu Foil Using Chemical Vapor Deposition. Nano Lett. 2012; 12: 161–66.

80. Chunyi Zhi,* Yoshio Bando, Chengchun Tang, Hiroaki Kuwahara, and Dimitri Golberg - Large-Scale Fabrication of Boron Nitride Nanosheets and Their Utilization in Polymeric Composites with Improved Thermal and Mechanical Properties. Adv. Mat. 2009; 21: 2889-93.

81. Yao, Y., Lin, Z., Li, Z., Song, X., Moon, K. S., Wong, C. P. Large-scale production of two-dimensional nanosheets. J. Mater. Chem. 2012; 22: 13494-99.

82. Li, L. H., Chen, Y., Behan, G., Zhang, H., Petravic, M., Glushenkov, A. M. Large-scale mechanical peeling of boron nitride nanosheets by low-energy ball milling. J. of mat. Chem. 2011; 21: 11862-66.

83. Jin C, Lin F, Suenaga K, Iijima S. Fabrication of a freestanding boron nitride single layer and its defect assignments. Phys. Rev. Lett. 2009; 102: 195505.

84. Meyer, J. C., Chuvilin, A., Algara-Siller, G., Biskupek, J., Kaiser, U. Selective sputtering and atomic resolution imaging of atomically thin boron nitride membranes, Nano Lett. 2009; 9:2683-89.

85. Nag, A., Raidongia, K., Hembram, K. P., Datta, R., Waghmare, U. V., Rao, C. N. R. Graphene Analogues of BN: Novel Synthesis and Properties, "ACS Nano 2010; 4: 1539-44.

86. Raidongia K, Nag A, Hembram KPSS, Waghmare UV, Datta R, Rao CNR. BCN: A Graphene Analogue with Remarkable Adsorptive Properties. Chem.Eur. J. 2010; 16: 149-57.

87. Tay, R. Y., Tsang, S. H., Loeblein, M., Chow, W. L., Loh, G. C., Toh, J. W., ... Teo, E. H. T. Direct growth of nanocrystalline hexagonal boron nitride films on dielectric substrates. Appl. Phys. Lett. 2015; 106: 101901.

88. Wang, X., Zhi, C., Li, L., Zeng, H., Li, C., Mitome, M., ... Bando, Y. "Chemical Blowing" of Thin-Walled Bubbles: High-Throughput Fabrication of Large-Area, Few-Layered BN and Cx-BN Nanosheets. Adv. Mate. 2011; 23: 4072-76.

89. Wang X, Pakdel A, Zhi C, Watanabe K, Sekiguchi T, Golberg D, Bando Y. High-yield boron nitride nanosheets from 'chemical blowing': towards practical applications in polymer composites. J. Phys.: Condens. Matter 2012; 24: 314205.

90. Han W, Bando Y, Kurashima K, Sato T. Synthesis of boron nitride nanotubes from carbon nanotubes by a substitution reaction. Appl. Phys. Lett. 1998; 73: 3085.

91. Golberg D, Bando Y, Kurashima K, Sato T. Ropes of BN multi-walled nanotubes. Solid State Commun. 2000 116: 1–6.

92Yurdakul, H., Göncü, Y., Durukan, O., Akay, A., Seyhan, A. T., Ay, N., Turan, S. Nanoscopic characterization of two-dimensional (2D) boron nitride nanosheets (BNNSs) produced by microfluidization. Ceram. Int. 2012; 38: 2187–93.

93. Golberg, D., Bando, Y., Eremets, M., Takemura, K., Kurashima, K., Yusa, H. Nanotubes in boron nitride laser heated at high pressure. Appl. Phys. Lett. 1996; 69: 2045.

94. Goldberg, D., Bando, Y., Eremets, M., Takemura, K., Kurashima, K., Tamiya, K., Yusa, H. Boron nitride nanotube growth defects and their annealing-out under electron irradiation. Chem. Phys. Lett. 1997; 279: 191-96.

95. Yu, D. P., Sun, X. S., Lee, C. S., Bello, I., Lee, S. T., Gu, H. D., ... Zhang, Z. Synthesis of boron nitride nanotubes by means of excimer laser ablation at high temperature. Appl. Phys. Lett. 1998; 72: 1966.

96. Lee, R. S., Gavillet, J., de La Chapelle, M. L., Loiseau, A., Cochon, J. L., Pigache, D., ... Willaime, F. Catalyst-free synthesis of boron nitride single-wall nanotubes with a preferred zig-zag configuration. Phys. Rev. B 2001; 64: 121405.

97. Zhang, Z., Guo, W., Dai, Y. Stability and electronic properties of small boron nitride nanotubes, J. Appl. Phys. 2009; 105: 084312.

98. Golberg, D.; Bando, Y.; Kurashima, K.; Sato, T. Synthesis and characterization of ropes made of BN multiwalled nanotubes. Scr. Mater. 2001, 44: 1561–64.

99. Li, C., Bando, Y., Zhi, C., Huang, Y., Golberg, D. Thickness-dependent bending modulus of hexagonal boron nitride nanosheets. Nanotechnology 2009; 20: 5707.

100. Bosak, A., Serrano, J., Krisch, M., Watanabe, K., Taniguchi, T., Kanda, H. Elasticity of hexagonal boron nitride: Inelastic x-ray scattering measurements. Phys. Rev. B 2006; 73: 041402.

101. Parashar A, Mertiny P, "Study of Mode I Fracture of Graphene Sheets Using Atomistic Based Finite Element Modeling and Virtual Crack Closure Technique. Int. J. Fract. 2012; 176: 119-26.

102. Li C, Tsu-Wei Chou TW. A structural mechanics approach for the analysis of carbon nanotubes. Int. J. Solids Struct. 2003; 40: 2487–99.

103.Tserpesa KI, Papanikosa P. Finite element modeling of single-walled carbon nanotubes, Composites Part B 2005; 36: 468–77.

104. Li C., Chou T.W. A structural mechanics approach for the analysis of carbon nanotubes. International Journal of Solids and Structures. 2003; 40: 2487-99.

105. Tserpesa K.I., Papanikosa P. Finite element modeling of single-walled carbon nanotubes Composites Part B: Engineering; 2005; 36:468-77.

106. Boldrin, L., Scarpa, F., Chowdhury, R., Adhikari, S. Effective mechanical properties of hexagonal boron nitride nanosheets. Nanotechnology 2011; 22: 505702.

107. Trivedi, S., Sharma, S. C., Harsha, S. P. Evaluations of Young's Modulus of Boron Nitride Nanotube Reinforced Nano-composites. Procedia Mater, Sci. 2014; 6: 1899–1905.

108. Trivedi, S., Sharma, S. C., Harsha, S. P. Dynamic Analysis of Single Walled Boron Nitride Nanotube Reinforced Composite Based Nanomechanical Resonator. Journal of the Institution of Engineers (India): Series D 2014; 95: 7-18.

109. Oh, E.S. Elastic properties of boron-nitride nanotubes through the continuum lattice approach, Mater. Lett. 2010; 64: 859–62.

110. Green, J. F., Bolland, T. K., Bolland, J. W. Lennard-Jones interaction for hexagonal layered crystals. J. Chem. Phys. 1974; 61: 1637.

111. Green, J. F., Bolland, T. K., Bolland, J. W. Theoretical elastic behavior for hexagonal boron nitride. J. Chem. Phys. 1976; 64: 656.

112. John P. Perdew and Yue Wang. Accurate and simple analytic representation of the electron-gas correlation energy. Phys. Rev. B 1992; 45:13244.

113. J. P. Perdew and Alex Zunger. Self-interaction correction to density-functional approximations for many-electron systems. Phys. Rev. B 1981; 23:5048.

114. John P. Perdew, Kieron Burke, and Matthias Ernzerhof, Generalized Gradient Approximation Made Simple. Phys. Rev. Lett. 1996; 77:3865.

115. Chengteh Lee, Weitao Yang, and Robert G. Parr. Development of the Colle-Salvetti correlation-energy formula into a functional of the electron density. Phys. Rev. B 1988 37:785.

116. Jianmin Tao, John P. Perdew, Viktor N. Staroverov, and Gustavo E. Scuseria, Climbing the Density Functional Ladder: Nonempirical Meta–Generalized Gradient Approximation Designed for Molecules and Solids. Phys. Rev. Lett. 2003; 91:146401.

117. John P. Perdew, Matthias Ernzerhof and Kieron Burke. Rationale for mixing exact exchange with density functional approximations. J. Chem. Phys. 1996 105:9982.

118. Carlo Adamo and Vincenzo Barone. Toward reliable density functional methods without adjustable parameters: The PBE0 model. J. Chem. Phys. 1999; 110:6158.

119. Baumeier, B., Krüger, P., Pollmann, J. Structural, elastic, and electronic properties of SiC, BN, and BeO nanotubes. Phys. Rev. B 2007; 76: 085407.

120. Ansari R., Malakpour S., Ajori S. Structural and elastic properties of hybrid bilayer graphene/h-BN with different interlayer distances using DFT. Superlattices Microstruct., 2014; 72: 230-37.

121. Topsakal, M., Aktürk, E., Ciraci, S. First-principles study of two- and one-dimensional honeycomb structures of boron nitride, Phys. Rev. B 2009; 79: 115442.

122. R. Ansari, S. Malakpour, M. Faghihnasiri and S. Ajori, Influence of Electric Field on the Mechanical Properties of Hexagonal Boron-Nitride Sheets Using ab-initio Calculations, NANO 10, 1550047 (2015).

123. Qing Peng, Wei Ji, Suvranu De. Mechanical properties of the hexagonal boron nitride monolayer: Ab initio study, Comput. Mater. Sci. Volume 56, April 2012, Pages 11–17.

124. Hernandez, E., Goze, C., Bernier, P., Rubio, A. Elastic properties of single-wall nanotubes. Appl. Phys. A 1999; 68: 287-92.

125. P. E. Blöchl. Projector augmented-wave method. Phys. Rev. B 1994; **50:**17953.

126. Topsakal M., Ciraci S. Elastic and plastic deformation of graphene, silicene, and boron nitride honeycomb nanoribbons under uniaxial tension: A first-principles density-functional theory study. Phys. Rev. B 2010; 81: 024107.

127. Baroni S., Giannozzi P., Isaev E. Density-Functional Perturbation Theory for Quasi Harmonic Calculation, Rev. Mineral. Geochem. 2010; 71: 39.

128. Mirnezhad M., Ansari R., Shahabodini A. Temperature Effect on Young's Modulus of Boron Nitride Sheets, J. Therm. Stresses; 2013 36: 152–159.

129. Tadmor E.B., E. MilleR E. Modeling Materials: Continuum, Atomistic and Multiscale Techniques, Cambridge University Press, 2012".

130. Swope, W. C., Andersen, H. C., Berens, P. H., Wilson, K. R. A computer simulation method for the calculation of equilibrium constants for the formation of physical clusters of molecules: Application to small water clusters. J. Chem. Phys. 1982; 76: 637.

131. Hockney R.W., Eastwood J.W. Computer Simulation Using Particles, McGraw-Hill, New York, 1981.

132. Beeman D. Some multistep methods for use in molecular dynamics calculations. J. Comput. Phys. 1976; 20: 130–39.

133. Tersoff J. New empirical model for the structural properties of silicon. Phys. Rev. Lett. 1986; 56: 632.

134. Tersoff J. New empirical approach for the structure and energy of covalent systems. Phys. Rev. B 1988; 37: 6991.

135. Tersoff J. Empirical Interatomic Potential for Carbon, with Applications to Amorphous Carbon. Phys. Rev. Lett. 1988; 61: 2869.

136. Tersoff J. Modeling solid-state chemistry: Interatomic potentials for multicomponent system. Phys. Rev. B 1989; 39: 5566.

137. Jones J.E. On the Determination of Molecular Fields. II. From the Equation of State of a Gas. Proc. R. Soc. London, Ser. A 1924; 106: 463-77".

138. Daw, M. S., Basks, M. I. Embedded-atom method: Derivation and application to impurities, surfaces, and other defects in metals. Phys. Rev. B 1984; 29, 6443.

139. Jeong, B. W., Lim, J. K., Sinnott, S. B. Tensile mechanical behavior of hollow and filled carbon nanotubes under tension or combined tension-torsion, Appl. Phys. Lett. 2007; 90: 023102.

140. Stuart, S. J., Tutein, A. B., Harrison, J. A. A reactive potential for hydrocarbons with intermolecular interactions, J. Chem. Phys. 2000; 112, 6472.

141. Singh, S. K., Neek-Amal, M., Costamagna, S., Peeters, F. M. Thermomechanical properties of a single hexagonal boron nitride sheets. Phys. Rev. B 2013; 87: 184106.

142. D.B. Zhang, E. Akatyeva, and T. Dumitrică, "Helical BN and ZnO nanotubes with intrinsic twisting: An objective molecular dynamics study. Phys. Rev. B 2011; 84: 115431.

143. Le M.Q. Prediction of Young's modulus of hexagonal monolayer sheets based on molecular mechanics. Int. J. Mech. Mater. Des. 2015; 11: 15-24.

144. Brenner D.W. Empirical potential for hydrocarbons for use in simulating the chemical vapor deposition of diamond films. Phys. Rev. B 1990; 42: 9458.

145. Sekkal W., Bouhafs B., Aourag H., Certier M. Molecular-dynamics simulation of structural and thermodynamic properties of boron nitride. J. Phys.: Condens. Matter 1998; 10: 4975.

146. Sevik, C., Kinaci, A., Haskins, J. B., Çağın, T. Characterization of thermal transport in low-dimensional boron nitride nanostructures, Phys. Rev. B 2011; 84: 085409.

147. Matsunaga K., Iwamoto Y. Molecular Dynamics Study of Atomic Structure and Diffusion Behavior in Amorphous Silicon Nitride Containing Boron. J. Am. Ceram. Soc. 2001; 84: 2213-19.

148. Matsunaga, K., Indra, Osamu H., Shoji I., Yasushi O. The new 5-HT 2A and analysis by receptor binding experiments and molecular modeling of the interaction with the receptor antagonist Nantenin the receptor. Japan pharmacology magazine 2000; 116: 48-52.

149. Matsunaga, K., Fisher, C., Matsubara, H. Tersoff Potential Parameters for Simulating Cubic Boron Carbonitrides. Jpn J. Appl. Phys. 2000; 39: 48.

150. Albe K., Möller W. Modeling of boron nitride: Atomic scale simulations on thin film growth. Comput. Mater. Sci. 1998; 10: 111–15.

151. Albe K., Möller W., Heinig K.H. Computer simulation and boron nitride. Radiat. Eff. Defects 1997; 141: 85-97.

152. Van Duin, A. C., Dasgupta, S., Lorant, F., Goddard, W. A. ReaxFF: A Reactive Force Field for Hydrocarbons. J. Phys. Chem. A 2001; 105: 9396–9409.

153. Weismiller, M. R., Duin, A. C. V., Lee, J., Yetter, R. A. ReaxFF Reactive Force Field Development and Applications for Molecular Dynamics Simulations of Ammonia Borane Dehydrogenation and Combustion. J. Phys. Chem. A 2010; 114: 5485–92.

154. Van Duin, A. C., Strachan, A., Stewman, S., Zhang, Q., Xu, X., Goddard, W. ReaxFFSiO Reactive Force Field for Silicon and Silicon Oxide Systems, J. Phys. Chem. A 2003; 107:3803-11.

155. Ohba, N., Miwa, K., Nagasako, N., Fukumoto, A. First-principles study on structural, dielectric, and dynamical properties for three BN polytypes. Phys. Rev. B 2001; 63: 115207.

156. Mirnezhad, M., Ansari, R., Rouhi, H. Mechanical properties of multilayer boron nitride with different stacking orders Super-lattices Microstruct. 2013; 53: 223–31.

157. Han, T., Luo, Y., Wang, C. Effects of temperature and strain rate on the mechanical properties of hexagonal boron nitride nanosheets. J. Phys. D: Appl. Phys. 2014; 47: 025303.

158. Wei, X., Wang, M. S., Bando, Y., Goldberg, D. Tensile Tests on Individual Multi-Walled Boron Nitride Nanotubes. Adv.Mater. 2010; 22: 4895-99.

159. Mortazavi, B., Rémond, Y. Investigation of tensile response and thermal conductivity of boron-nitride nanosheets using molecular dynamics simulations. Physica E 2012; 44: 1846-52.

160. Zhao, S., Xue, J. Mechanical properties of hybrid graphene and hexagonal boron nitride sheets as revealed by molecular dynamic simulations, J. Phys. D: Appl. Phys. 2013; 46: 135303.

161. Le, M. Q., Nguyen, D. T. Atomistic simulations of pristine and defective hexagonal BN and SiC sheets under uniaxial tension. Mater. Sci. Eng. A, 2014; 615: 481–88.

162. Yuan, J.; Liew, K. M. The Effects of Grafted Carboxyl Groups on the Elastic Properties of Single-Walled Boron Nitride Nanotubes. J. Comput. Theor. Nanosci.2010; 7: 1878-84.

163. Ghazizadeh M., Estevez J.E, Kelkar A.D., Ryan J.G. Mechanical Properties Prediction of Hydrogenated Boron Nitride Nanotube's using Molecular Dynamic Simulations, JSM Nanotechnol Nanomed 2014; 2: 1030.

164. Rappé, A. K., Casewit, C. J., Colwell, K. S., Goddard Iii, W. A., Skiff, W. M. UFF, a full periodic table force field for molecular mechanics and molecular dynamics simulations. J. Am. Chem. Soc. 1992; 114: 10024-35.

165. T.A. Hilder, R. Yang, V. Ganesh, D. Gordon, A. Bliznyuk, A.P. Rendell, S.H. Chung. Validity of current force fields for simulations on boron nitride nanotubes. Micro & Nano Letters, 2010; 5:150-156.

166. Han S. S., Kang JK, Leea HM. The theoretical study on interaction of hydrogen with single-walled boron nitride nanotubes. I. The reactive force field ReaxFFHBN development. J. Chem. Phys. 2005; 123:114703.

166. Srivastava, D., Menon, M., Cho, K. Anisotropic nanomechanics of boron nitride nanotubes: Nanostructured "skin" effect. Phys. Rev. B 2001; 63: 195413.

167. Ebrahimi-Nejad, S., Shokuhfar, A. Compressive buckling of open-ended boron nitride nanotubes in hydrogen storage applications. Physica E 2013; 50: 29–36.

168. Liao, M. L., Wang, Y. C., Ju, S. P., Lien, T. W., Huang, L. F. Deformation behaviors of an armchair boron-nitride nanotube under axial tensile strain. J. Appl. Phys. 2011; 110: 054310.

169. Shen H.J. Mechanical properties and electronic structures of one BN nanotube under radial compression. Front. Mater. Sci. China 2009; 3: 201-04.

170. Ebrahimi-Nejad, S., Shokuhfar, A., Zare-Shahabadi, A. Molecular Dynamics Simulation of the Buckling Behavior of Boron Nitride Nanotubes under Uniaxial Compressive Loading. Defect and Diffusion Forum 2010; 297: 984-89.

171. Slotman G.J., Fasolino A. Structure, stability and defects of single layer hexagonal BN in comparison to graphene. J. Phys.: Condens. Matter 2013; 25: 045009.

172. Liao, M. L., Lian, T. W., Ju, S. P. Tensile and Compressive Behaviors of a Boron Nitride Nanotube: Temperature Effects. Mater. Sci. Forum 2012; 700: 125-28.

173. Shokuhfar, A., Ebrahimi-Nejad, S., Hosseini-Sadegh, A., Zare-Shahabadi, A. The effect of temperature on the compressive buckling of boron nitride nanotubes. physica status solidi (a) 2012; 209: 1266-73.

174. Yuan, J., Liew, K. M. High-Temperature Thermal Stability and In-Plane Compressive Properties of a Graphene and a Boron-Nitride Nanosheet. J. Nanosci. Nanotechnol. 2012; 12: 2617-24.

175. Zobelli, A., Ewels, C. P., Gloter, A., Seifert, G., Stephan, O., Csillag, S., Colliex, C. Defective Structure of BN Nanotubes: From Single Vacancies to Dislocation Lines. Nano Lett. 2006; 6: 1955–60.

176. Stone A.J., Wales D.J. Theoretical studies of icosahedral C60 and some related species, Chem.l PhY. Lett. 1986; 128: 501-03.

177. Griebel, M., Hamaekers, J., Heber, F. A molecular dynamics study on the impact of defects and functionalization on the Young modulus of boron–nitride nanotubes. Comput.Mater.Sci. 2009; 45: 1097–1103.

178. Parrinello M., A. Rahman A. Polymorphic transitions in single crystals: A new molecular dynamics method, J. Appl. Phys. 1981; 52: 7182.

179. Shokuhfar, A., Ebrahimi-Nejad, S. Effects of structural defects on the compressive buckling of boron nitride nanotubes. Physica E 2013; 48: 53–60.

180. Sarma, J. V. N., Chowdhury, R., Jayaganthan, R., Scarpa, F. Atomistic Studies on Tensile Mechanics of BN Nanotubes in the Presence of Defects. Int. J. Nanosci.2014; 13: 1450005.

181. Krishnan N.M.A., Debraj Ghosh D. Defect induced plasticity and failure mechanism of boron nitride nanotubes under tension. J. Appl. Phys. 2014; 116: 044313.

182. Mortazavi B., Cunibertiabcd G. Mechanical properties of polycrystalline boron-nitride nanosheets. RSC Adv. 2014; 4: 19137-43.

183. Moon W.H., Hwang H.J. Molecular-dynamics simulation of structure and thermal behaviour of boron nitride nanotubes. Nanotechnology 2004; 15: 431.

184. Wei R., Tian Y., Eichhorn V., Fatikow S. Compressive and tensile behaviors of carbon and boron nitride nanotubes. Manipulation, Manufacturing and Measurement on the Nanoscale (3M-NANO) 2012:301-04.

185. Tian, Y., Li, Z., Gao, W., Cai, K., Wang, F., Zhang, D., ... Fatikow, S. Mechanical properties investigation of monolayer h-BN sheet under in-plane shear displacement using molecular dynamics simulations. J. Appl. Phys. 2014; 115: 014308.

186. Perim, E., Santos, R. P., Autreto, P. A. D. S. Galvao, D. S. Fracture Patterns of Boron Nitride Nanotubes. MRS Proceedings 2013; 1526.

187. Krishnan N.M.A., Ghosh D. Chirality dependent elastic properties of single-walled boron nitride nanotubes under uniaxial and torsional loading. J. Appl. Phys. 2014; 115: 064303.

188. Ansari A., Ajori S. Molecular dynamics study of the torsional vibration characteristics of boron-nitride nanotubes, Physics Letters A, 2014; 378: 2876-80.

189. Ajori S., Ansari R. Torsional buckling behavior of boron-nitride nanotubes using molecular dynamics simulations. Curr. Appl Phys. 2014; 14: 1072-77.

190. Le M.Q. Size effects in mechanical properties of boron nitride nanoribbons. J. Mech. Sci. Technol. 2014; 28: 4173-78.

191. Tang, D. M., Ren, C. L., Wei, X., Wang, M. S., Liu, C., Bando, Y., Golberg D. Mechanical Properties of Bamboo-like Boron Nitride Nanotubes by In Situ TEM and MD Simulations: Strengthening Effect of Interlocked Joint Interfaces. ACS Nano 2011; 5: 7362–68.

192. Chaddertona L.T., Chenb Y. A model for the growth of bamboo and skeletal nanotubes: catalytic capillarity. J. of Cryst. Growth 2002; 240: 164-69.

193. Tang, D. M., Liu, C., Cheng, H. M. Controlled synthesis of quasi-one-dimensional boron nitride nanostructures. J. Mater. Res. 2007; 22: 2809-16.

194. Shen H.J. Thermal-conductivity and tensile-properties of BN, SiC and Ge nanotubes. Comput. Mater. Sci. 2009; 47: 220-24.

195. Kınacı, A., Haskins, J. B., Sevik, C., Çağın, T. Thermal conductivity of BN-C nanostructures. Phys. Rev. B 2012; 86: 115410.

196. Lindsay L., Broido D.A. Optimized Tersoff and Brenner empirical potential parameters for lattice dynamics and phonon thermal transport in carbon nanotubes and graphene. Phys. Rev. B 2010; 81:205441.

197. Chen, Y. C., Lee, S. C., Liu, T. H., Chang, C. C. Thermal conductivity of boron nitride nanoribbons: Anisotropic effects and boundary scattering. Int. J. Therm. Sci. 2015; 94: 72–78.

198. Muller-Plathe F. A simple nonequilibrium molecular dynamics method for calculating the thermal conductivity. J. Chem. Phys. 1997; 106: 6082.

199. Sevik, C., Kinaci, A., Haskins, J. B., Çağın, T. Influence of disorder on thermal transport properties of boron nitride nanostructures. Phys. Rev. 2012; B 86, 075403.

200. Shen H.J. The Effects of Radial Compression on Thermal Conductivity of Carbon and Boron Nitride Nanotubes. Journal of Nanomaterials 2012; 756791.

201. Mashreghi A. Thermal expansion/contraction of boron nitride nanotubes in axial, radial and circumferential directions. Comput. Mater. Sci. 2012; 65: 356-64.

202. Liew K.M., Yuan J. High-temperature thermal stability and axial compressive properties of a coaxial carbon nanotube inside a boron nitride nanotube. Nanotechnology 2011; 22: 085701.

203. Rappe, A. K., Colwell, K. S., Casewit, C. J. Application of a universal force field to metal complexes, Inorg. Chem. 1993; 32: 3438-50.

204. Yuan J., Liao J., Yang C., Shi X. Structural Stability and Elastic Properties of Bilayer Graphenes and Boron Nitride Nanosheets. Current Nanoscience 2013; 9: 324-29.

205. Yuan J., Liew K.M. Structure stability and high-temperature distortion resistance of trilayer complexes formed from graphenes and boron nitride nanosheets. Phys. Chem. Chem. Phys. 2014; 16: 88-94.

206. Song J., Nikhil V Medhekar N.V. Thermal transport in lattice-constrained 2D hybrid graphene heterostructures, J. Phys.: Condens. Matter 2013; 25: 445007.

207. Shen H.J. Thermal-stability and compressive properties of one boron nitride nanotube embedded in another carbon tube. Micro Nano Lett. 2011; 6: 444-47.

208. Zhang G., Zhoubc R., Zeng X.C. Carbon nanotube and boron nitride nanotube hosted C60–V nanopeapods. J. Mater. Chem. C 2013; 1:4518-26.

209. Nasrabadi A.T., Foroutan M. Interactions between Polymers and Single-Walled Boron Nitride Nanotubes: A Molecular Dynamics Simulation Approach. J. Phys. Chem. B 2010; 114: 15429-36.

210. Allinger N.L., Yuh Y.H., Lii J.H. Molecular mechanics. The MM3 force field for hydrocarbons, J. Am. Chem. Soc. 1989; 111: 8551-66.

211. Fatemi S.M., Foroutan M. Study of dispersion of boron nitride nanotubes by triton X-100 surfactant using molecular dynamics simulations. J. Theor. Comput. Chem. 2014; 13: 1450063.

212. Frisch M.J., Trudes G.W., Schlegel H.B. Gaussian 03, Revision C.02, Gaussian Inc., Wallingford, CT, 2004.

213. Wang, J., Li, H., Li, Y., Yu, H., He, Y., Song, X. Deformation of copper-filled single-walled boron-nitride nanotubes under axial compression, Physica E: Low-dimensional Systems and Nanostructures 2011; 44: 286-89.

214. Jung, D. H., Kim, D., Lee, T. B., Choi, S. B., Yoon, J. H., Kim, J., ... Choi, S. H. Grand Canonical Monte Carlo Simulation Study on the Catenation Effect on Hydrogen Adsorption onto the Interpenetrating Metal−Organic Frameworks. J. Phys. Chem. B 2006; 110: 22987-90.

215. Zhou, Y., Adams, S., Rao, R. P., Edwards, D. D., Neiman, A., Pestereva, N. Charge Transport by Polyatomic Anion Diffusion in Sc2(WO4)3. Chem. Mater. 2008; 20: 6335-45.

216. Bari, R., Parviz, D., Khabaz, F., Klaassen, C. D., Metzler, S. D., Hansen, M. J., ... Green, M. J. Liquid phase exfoliation and crumpling of inorganic nanosheets. Phys. Chem. Chem. Phys. 2015; 17: 9383-93.

217. Wang J, Wolf R.M., Caldwell J.W., Peter A. Kollman P.A., David A. Development and testing of a general amber force field. J. of Computa. Chem. 2004: 25:1157-74.

218. Wanga J, Wangb W, Kollmanc P.A., David A. Automatic atom type and bond type perception in molecular mechanical calculations. J. of Molecular Graphics and Modeling 2006; 25:247-60.

219. Mayo S.L., Olafson B.D., Goddard W.A. DREIDING: a generic force field for molecular simulations. J. Phys. Chem. 1990; 94:8897–8909.

220. Griebel M., Hamaekers J. Molecular dynamics simulations of boron-nitride nanotubes embedded in amorphous Si-B-N. Comput. Mate. Sci. 2007; 39: 502-17.

221. Parrinello M. Rahman A. Crystal Structure and Pair Potentials: A Molecular-Dynamics Study, Phys. Rev. Lett. 1980; 45: 1196.

222. Thomas M., Enciso M., Hilder T.A. Insertion Mechanism and Stability of Boron Nitride Nanotubes in Lipid Bilayers. J. Phys. Chem. B 2015; 119: 4929-36.

223.MacKerell, A. D., Bashford, D., Bellott, M. L. D. R., Dunbrack, R. L., Evanseck, J. D., Field, M. J., … Karplus, M. (All-Atom Empirical Potential for Molecular Modeling and Dynamics Studies of Proteins. J. Phys. Chem. B 1998; 102: 3586-16.

224. MacKerell, A. D., Feig, M., Brooks, C. L. extending the treatment of backbone energetics in protein force fields: Limitations of gas-phase quantum mechanics in reproducing protein

conformational distributions in molecular dynamics simulations, J. Comput. Chem.2004; 25: 1400-15.

225. Yuan J., Liew K.M. Formation and Compressing Behavior of Coaxial Silicon Nanowires inside a Boron Nitride Nanotube. J. Phys. Chem. C 2011; 115: 431-35.